

N93-16538

Unclas

G3/02 0136506

11-15-92
13-1-96
0 77

**PARTICLE KINETIC SIMULATION
OF HIGH ALTITUDE HYPERVELOCITY FLIGHT**

Periodic Research Report
Cooperative Agreement NCC2-582

for the period
February 1, 1992 - December 31, 1992

Submitted to

National Aeronautics and Space Administration
Ames Research Center
Moffett Field, California 94035

Aerothermodynamics Branch
Dr. George S. Deiwert, Chief and Technical Officer

Thermosciences Division
Dr. Jim Arnold, Chief

Prepared by

ELORET INSTITUTE
1178 Maraschino Drive
Sunnyvale, CA 94087
Phone: 408 730-8422 and 415 493-4710
Telefax: 408 730-1441

Dr. K. Heinemann, President and Grant Administrator
Dr. Iain D. Boyd, Principal Investigator
Dr. Brian L. Haas, Co-Principal Investigator

4 January, 1993

(NASA-CR-191628) PARTICLE KINETIC
SIMULATION OF HIGH ALTITUDE
HYPERVELOCITY FLIGHT Progress
Report, 1 Feb. - 31 Dec. 1992
(Eloret Corp.) 77 p

416

Summary

In this grant period, the focus has been on the effects of thermo-chemical nonequilibrium in low-density gases, and on interactions between such gases and solid surfaces. Such conditions apply to hypersonic flows of re-entry vehicles, and to the expansion plumes of small rockets. Due to the nonequilibrium nature of these flows, a particle approach has been adopted. The method continues to undergo refinement and application to typical flows of interest.

A number of studies have been performed for flows in thermo-chemical nonequilibrium. The effects of vibrational nonequilibrium on the rate of dissociation were studied for diatomic nitrogen. It was found that a new model reproduced the nonequilibrium behavior observed experimentally. This work is described in Appendix A: a reprint from the Physics of Fluids. A further study made comparison between the chemistry models employed in particle and more traditional continuum computational methods. It was found that the 2 approaches did give good agreement under conditions favorable to the continuum approach: this investigation is included in Appendix B which is a preprint

for an article to be published in the Journal of Thermophysics and Heat Transfer. Finally, a study has been completed which considers the effects of using particle methods to predict the radiative emission produced in strong shock-waves in air. In comparisons of particle and continuum results, the total radiative intensity was found to be the same, although details in the profiles showed significant differences. This work was reported at the AIAA 23rd Plasmadynamics Conference in Nashville, July 1992 and is included as Appendix C.

The particle method was used for analysis of aerodynamic torques for stability of the Magellan spacecraft entering the atmosphere of Venus at non-zero pitch and yaw at hypersonic, rarefied conditions. This work is submitted for presentation at the AIAA Atmospheric Flight Mechanics Conference, August 1993 (see Appendix D). New models were developed for computing vehicle surface temperatures directly in the particle simulation which account for surface radiation, heat capacity and conductivity of the material, and the transient nature of the aerodynamic heating pulse during aerobraking. This work was presented at the 18th International Symposium on Rarefied Gas Dynamics in Vancouver, Canada, July 1992 (see Appendix E). A parametric study was initiated which determines the accuracy

of particle flow solutions over a wide range of Mach number, Knudsen number, and wall temperature for Hard-sphere and Maxwell molecules, depending upon the grid resolution and flow domain employed in the simulation. This work is submitted for presentation at the AIAA 28th Thermophysics Conference, July 1993 (see Appendix F).

APPENDIX A

Analysis of vibration-dissociation-recombination processes behind strong shock waves of nitrogen

Iain D. Boyd^{a)}

Eloret Institute, 3788 Fabian Way, Palo Alto, California 94303

(Received 9 April 1991; accepted 23 July 1991)

Computations are presented for the relaxation zone behind strong, one-dimensional shock waves of nitrogen. The numerical results are compared with existing experimental data. It is indicated that the derivation of chemical rate coefficients must account for the degree of vibrational nonequilibrium in the flow. A nonequilibrium chemistry model is employed together with equilibrium rate data to compute successfully the flow in several different nitrogen shock waves. The analysis is performed with the direct simulation Monte Carlo method (DSMC). The DSMC code is vectorized for efficient use on a supercomputer. The code simulates translational, rotational, and vibrational energy exchange, and dissociative and recombinative chemical reactions. A new model is proposed for the treatment of three-body recombinative collisions in the DSMC technique, which usually simulates binary collision events. The new formulation represents improvement over previous models in that it can be employed with a wide range of chemical rate data, does not introduce into the flow field troublesome pairs of atoms that may recombine upon further collision (pseudoparticles), and is compatible with the vectorized code.

I. INTRODUCTION

The direct simulation Monte Carlo method (DSMC) developed extensively by Bird (Ref. 1, Chap. 7) is a powerful technique for simulating flows of rarefied gases. The method simulates the gas flow as a collection of model particles that move through physical space undergoing the intermolecular collisions and boundary interactions appropriate to the local flow conditions. Collisions are simulated on a statistical rather than deterministic basis, and local conditions are captured by dividing physical space into a network of cells. The numerical expense of the technique is directly proportional to the density of the flow that has restricted its application to flows in the transitional regime lying between continuum and free molecular.

Because of the relative computational simplicity of the one-dimensional normal shock wave, this problem provides an opportunity to extend the use of the DSMC method into the continuum regime. Previously, DSMC has been employed in normal shock waves to study translational,² rotational,³ and vibrational nonequilibrium.⁴ Earlier, the computation of dissociating nitrogen shock waves was performed by Bird.⁵ However, this study involved a finite-difference type approach to the problem in which constant volume relaxation was performed in each computational cell. By comparing the simulated results with the corresponding finite difference expressions, the values of temperature, density, and velocity were adjusted in each cell over each time step. This rather cumbersome procedure was adopted because of the severe computational penalty associated with performing a full DSMC calculation of the flow. One of the purposes of this paper is to report upon the devel-

opment of a DSMC code that simulates chemical reactions and is highly vectorized for efficient performance on supercomputers. The speed-up attained through vectorization allows the proper computation of normal shock waves with the DSMC technique. For compatibility with the vectorized procedures, a new model for simulating three-body recombination reactions in the DSMC technique is introduced. The new model is described, and will be shown to have several advantages over the previous recombination procedures. The flow conditions of the shock waves computed in this study have been chosen to correspond to some of those investigated previously in the literature.

II. VECTORIZED IMPLEMENTATION OF PHYSICAL MODELS

As described by Bird (Ref. 1, Chap. 7), the DSMC algorithm consists of moving the particles, sorting the particles, colliding the particles, and sampling the properties of the particles. A vectorized implementation of the DSMC algorithm for a single-species gas has been described by Boyd.⁶ The performance attained with this implementation is equal to that first reported for such particle methods by Baganoff and McDonald.⁷ For the computation of reacting shock waves, this implementation must be extended to simulate a mixture of gases, and to include the additional collision events of vibrational energy exchange, and dissociative and recombinative chemical reactions.

Vectorized implementations of the tasks performed in the DSMC algorithm are provided by Boyd.⁶ Of these, only the implementation for the sampling of the particle properties must be revised for the simulation of a multispecies gas mixture. In the new implementation, a loop is made over the total number of simulated particles. For each of these parti-

^{a)} Mailing address: NASA Ames Research Center, MS 230-2, Moffett Field, California 94035.

cles, the current computational cell and species numbers are identified. Then, several counters are updated for that particular cell and species. These counters consist of the individual velocity components, the squares of the velocity components (these two quantities are employed in the evaluation of translational temperature), the rotational and vibrational energies, and the number of particles sampled. If the particles are sufficiently well mixed within the simulation, then vectorization of this implementation works perfectly. However, should two particles of the same species and cell number occur over the same vector length, then only the properties of the latter molecule will be recorded. While this means that the information of the first particle is lost, this aspect does not lead to any error. The number density in each cell is recorded accurately as the sorting algorithm produces this information.

The vectorized shock code simulates a number of different collisional phenomena: translational, rotational, and vibrational energy exchange; dissociative and recombinative chemical reactions. The total number of collisions that exchange translational energy is governed by the no-time-counter technique.⁸ The number of these collisions that undergo rotational energy exchange is given by the expression developed by Boyd.³ In a revised form, this probability is expressed as a function of the sum of the translational and rotational collision energies. This aspect permits instantaneous evaluation⁹ thus providing compatibility with the vectorized implementation.

The rate of exchange of energy involving the vibrational modes is simulated through application of a variable probability that consists of two separate components.¹⁰ The first is derived from the Millikan and White¹¹ experimental correlation for the vibrational relaxation time τ_1 , and is given by

$$P_{v1} = \frac{1}{\nu\tau_1} = \frac{1}{Z_1} g^{3+2\omega} \exp\left(\frac{-g^*}{g}\right), \quad (1)$$

where ν is the collision rate, g is the relative collision velocity, and ω determines the nature of the interaction potential in the variable hard sphere (VHS) collision model.¹² The constants Z_1 and g^* are chosen to match the experimental correlation for the vibrational relaxation time. For nitrogen, this probability becomes unrealistically high at temperatures greater than about 10 000 K. To simulate the relaxation time at such elevated temperatures, an empirical correction term τ_2 is added to the relaxation time, where

$$P_{v2} = 1/\nu\tau_2 = (1/Z_2)g^{2\omega}. \quad (2)$$

The value for Z_2 for nitrogen is obtained by Haas and Boyd.¹³ The overall exchange probability is then given as

$$P_v = \frac{1}{\nu(\tau_1 + \tau_2)} = \frac{1}{1/P_{v1} + 1/P_{v2}}. \quad (3)$$

At low temperatures, the second term tends to zero, and the vibrational relaxation time is given by the Millikan and White expression. Conservely, at high temperatures, the second term dominates.

As the vibrational energy exchange probability is not a function of the sum of the translational and vibrational energies, the probability should not be evaluated instantaneous-

ly. Therefore the values of P_{v1} and P_{v2} must be obtained by averaging over all collisions. In the vectorized implementation, an average vibrational exchange probability is assigned to each computational cell. The probability is updated by employing the relative velocity of every collision that occurs in each cell over each time step. This process is performed after the pairing of collision pairs, but before computation of the collision mechanics, and is fully vectorized.

The mechanisms of both rotational and vibrational energy exchange follow the usual model of Borgnakke and Larsen,¹⁴ and are processed efficiently using precomputed lookup tables. It has been observed in a recent study by Lumpkin *et al.*¹⁵ that the mechanisms of energy transfer employed in the DSMC technique affect the rate of energy transfer. For the collision number of an internal mode, the precise relationship between DSMC and continuum definitions is given in Ref. 15. It is shown that the value of the collision number used in DSMC will be approximately half of that determined experimentally and employed in a continuum or kinetic computation. These adjustments have been included in the probabilities of energy transfer to the rotational and the vibrational modes.

The chemistry model employed in the study is the vibrationally-favored dissociation (VFD) model of Haas and Boyd.¹³ The rate of dissociation is governed by a set of chemical rate coefficients that are reproduced in the simulation under conditions of equilibrium. The model also simulates the important physical phenomenon of coupled vibration dissociation. This causes a reduction in the rate of dissociation when the vibrational energy mode is out of equilibrium with the translational and rotational modes, which often occurs behind strong shock waves. The dissociation probability takes the form

$$P_d = (1/Z_d) [(E_c - E_a)^{\psi_1}/E_c^{\psi_2}] E_v^\phi, \quad (4)$$

where E_c is the total collision energy, E_a is the activation energy of the reaction, and E_v is the vibrational energy of the reacting molecule. The constant ϕ determines the degree of vibration-dissociation coupling, and the other constants, Z_d , ψ_1 , and ψ_2 , are determined from molecular constants, the chemical rate data, and the value of ϕ . By matching dissociation incubation distances observed experimentally to simulated data, the appropriate value for nitrogen was established by Haas and Boyd¹³ as $\phi = 3$. For compatibility with the VFD model and the vectorized implementation, it was necessary to develop a new model for simulating recombination reactions in the DSMC technique. This model is described in the following section.

The vectorized implementation of these physical models proceeds by constructing lists of pairs of molecules that undergo different collisional events. Initially, a list of possible collision candidates is formed; then a list of those that do collide. The pairs of molecules that collide are then subdivided into lists of those that dissociate, those that recombine, those that exchange vibrational energy, those that exchange rotational energy, and the remainder just exchange translational energy. The list formed of particles that experience each of these phenomena are then processed in computationally efficient, vectorized loops. Finally, the collision me-

chanics of all the molecules that collide are processed in a vectorized loop. A symbolic representation of the vectorized implementation of the collision algorithm is given in Fig. 1. Each of the statements represents one loop; or a set of nested loops in the code. Of the eleven such loops, only that entitled "Create List Of Pairs Of Molecules" is not fully vectorized. The vectorized coding provides a speed-up by a factor of 10 in comparison with the scalar implementation of the algorithm.

III. RECOMBINATION MODEL

In the DSMC technique, collisions are usually considered between just two molecules. It therefore represents a challenge to simulate three-body recombination reactions. The first such model incorporated into the DSMC technique was proposed by Bird.⁵ In this model, a lifetime was assigned to a binary pair, and a three-body collision treated as a further collision with this intermediary, pseudoparticle. This scheme requires a number of assumptions to be made concerning the relationships between the various three-body collision cross sections, and the model does not lend itself readily to inclusion in the no-time-counter collision scheme. Also, under exceptional conditions, the lifetimes assigned to the intermediary pair can be very large, such that the pseudoparticle remains in the flow field for a considerable time. This result is physically unrealistic, and computationally troublesome. An improved recombination model was proposed by Haas¹⁶ for use in the particle method of Baganoff and McDonald.⁷ In this model, the pseudoparticles are created at one time step, and then are either recombined or are split apart into the constitutive atoms on the following time step. While the scheme may be successfully incorporated into a vectorized implementation, it still has the disadvantage of producing pseudoparticles that must be processed by the whole algorithm (in this case, just for one time step). This requirement stems from the structure of the algorithm proposed by Baganoff and McDonald. A further disadvantage of this model is that it requires assumptions to be made for the form of the molecular interaction involving the pseudomolecule. The objective of the present model is to remove

the troublesome elements of the method developed by Haas, while retaining the ability to vectorize the algorithm.

In Vincenti and Kruger,¹⁷ it is stated that, for the recombination reaction between two nitrogen atoms and any third body M ,



the rate of formation of N_2 is governed by

$$\frac{dn_{N_2}}{dt} = (k_b n_N n_N) n_M, \quad (6)$$

where n_N and n_M are the number densities of atomic nitrogen and the third body M and k_b is the backward (recombination) rate coefficient. This term is related to the forward (dissociation) rate coefficient k_f and the equilibrium constant K_c in the following way:

$$k_b = k_f / K_c = (a_f / a_c) T^{b_f - b_c}, \quad (7)$$

where T is the temperature, a_f and b_f are the rate parameters associated with the forward reaction, and a_c and b_c are those associated with the equilibrium constant. The parentheses in Eq. (6) indicate that, in the new recombination model for the DSMC technique, the reaction is first treated as a binary collision between two atoms. This allows the derivation of a recombination probability in the same way as for a dissociating reaction. To reproduce the correct rate of recombination, the probability must then be multiplied by the number density n_M . The task for implementing this process in a DSMC simulation is to relate the rate coefficient k_b to a probability of recombination P_r . This probability is expressed as a function of the collision energy E_c . When this probability is integrated over all collision energies, and then multiplied by the collision rate, it must lead to the value of the backward rate coefficient at a particular temperature. Simplification of this analysis leads to the following expression:

$$\frac{a_f}{a_c} T^{b_f - b_c} = n_M \overline{\sigma g} \int_0^\infty P_r(E_c) f\left(\frac{E_c}{kT}\right) d\left(\frac{E_c}{kT}\right), \quad (8)$$

where σ is the collision cross section for atom-atom collisions, and g is the relative velocity of collision. In the new model, the possibility of recombination is assessed only when two atoms collide. A third colliding body (either atom or molecule) is then chosen at random to complete the ternary collision. As the third colliding body is chosen randomly from those that exist in the cell, the recombination rate is achieved in the simulation by multiplying the probability by the total number density instead of n_M . In this implementation, the total collision energy E_c is comprised of two components. The first, E_t , is the collision energy of the two colliding atoms. The equilibrium distribution of this energy for the VHS intermolecular potential is

$$f\left(\frac{E_t}{kT}\right) = \frac{1}{\Gamma(2 - \omega)} \left(\frac{E_t}{kT}\right)^{1 - \omega} \exp\left(-\frac{E_t}{kT}\right). \quad (9)$$

When the two atoms come together, they form a pseudoparticle and their center of mass velocity is then collided with a third body to determine if recombination actually occurs. Bird (Ref. 1, Chap. 12) shows that the distribution function

```

Symbolic Vectorized Implementation of DSMC Collision Algorithm.

Compute_Number_Of_Collisions_Per_Cell_According_To_MTC_Scheme
Create_List_Of_Pairs_Of_Molecules
Create_Sublist_Of_Molecules_Which_Collide
With_Sublist_Update_Average_Vibrational_Exchange_Probabilities_Per_Cell
With_Sublist_Create_Sublist1_Of_Molecules_Which_Dissociate
                                Sublist2              _Recombine
                                Sublist3              _Exchange_Vibrational_Energy
                                Sublist4              _Exchange_Rotational_Energy

With_Sublist1_Perform_Dissociating_Reactions
With_Sublist2_Perform_Recombining_Reactions
With_Sublist3_Perform_Vibrational_Energy_Exchange
With_Sublist4_Perform_Rotational_Energy_Exchange
With_Sublist_Perform_Mechanics_For_All_Colliding_Pairs

```

FIG. 1. Symbolic vectorized implementation of DSMC collision algorithm.

of the center of mass velocity for the two atoms is just the thermal velocity distribution of the combined molecule. No selection criteria are applied to the collision between the third body and the pseudoparticle as the body is chosen at random. Thus the distribution function of the collision energy E_x for the pseudoparticle and a third body is just that for three degrees of freedom in translational energy, and ζ degrees of freedom in internal energy:

$$f\left(\frac{E_x}{kT}\right) = \frac{1}{\Gamma(3/2 + \zeta/2)} \left(\frac{E_x}{kT}\right)^{1/2 + \zeta/2} \exp\left(-\frac{E_x}{kT}\right). \quad (10)$$

To obtain the distribution for the total collision energy $E_c = E_t + E_x$, it is necessary to multiply Eqs. (9) and (10) together and then to integrate over either variable. The result of this analysis is

$$f\left(\frac{E_c}{kT}\right) = \frac{1}{\Gamma(7/2 + \zeta/2 - \omega)} \left(\frac{E_c}{kT}\right)^{5/2 + \zeta/2 - \omega} \times \exp\left(-\frac{E_c}{kT}\right). \quad (11)$$

For mathematical convenience, the form of the recombination probability is chosen as

$$P_r(E_c) = (1/Z_r) E_c^\chi. \quad (12)$$

Then, substituting into Eq. (8) and integrating, it is found that the following result gives the correct temperature dependence of the backward rate coefficient:

$$\chi = b_f - b_c - 1/2 + \omega \quad (13)$$

and

$$\frac{1}{Z_r} = \frac{\sqrt{\pi}}{2^{1/2 - \omega}} \frac{a_f/a_c}{k^{b_f - b_c}} \frac{m_r^{1/2 - \omega}}{\sigma_0} \times \left(\frac{m_r}{2(2 - \omega)kT_0}\right)^\omega \frac{\Gamma(7/2 + \zeta/2 - \omega)}{\Gamma(7/2 + \zeta/2 - \omega + \chi)}, \quad (14)$$

where m_r is the reduced mass of the atom-atom collision, and σ_0 is a reference cross section for the atom-atom collision at temperature T_0 in the VHS collision model. The value of χ employed in the simulation must satisfy the restriction that the arguments of the gamma functions must be greater than zero. This is satisfied by all of the combinations of the values of b_f and b_c found for nitrogen in the literature.

In the implementation of the recombination probability P_r , a multiplying factor of 100 or 1000 is usually employed, and subsequently the recombination probability is only assessed every 1/100 or 1/1000 times that two atoms collide. This procedure is adopted due to the relative infrequency of recombination reactions in most flows of interest, and thus represents a more numerically efficient manner to treat the problem.

IV. RESULTS AND DISCUSSION

The first test of the recombination model is performed under equilibrium conditions. At a constant temperature and density, the model must reproduce the theoretical value for the average recombination probability. The results of an

equilibrium study are shown in Fig. 2. The simulation conditions were $\rho = 3 \text{ kg m}^{-3}$, $T = 10\,000 \text{ K}$, and the mass fraction of atomic nitrogen $\alpha = 0.65$. Time is normalized through division by the mean time between collisions. The recombination rate coefficients were determined from the following rate data:

$$k_f(N_2 - N_2) = 7.97 \times 10^{-13} T^{-0.5} \times \exp(-113\,200/T) \text{ m}^3/\text{molecule}/\text{sec}, \quad (15a)$$

$$k_f(N_2 - N) = 7.14 \times 10^{-8} T^{-1.5} \times \exp(-113\,200/T) \text{ m}^3/\text{molecule}/\text{sec}, \quad (15b)$$

$$K_c(N_2) = 1.084 \times 10^{31} \exp(-113\,200/T) \text{ molecule}/\text{m}^3. \quad (15c)$$

The dissociation rate coefficients are due to Byron¹⁸ and the equilibrium constant is taken from Vincenti and Kruger.¹⁷ It is shown that the model described in the previous section does produce the average probability of recombination predicted by theory.

The next test is to ensure that the dissociation and recombination models allow a stationary gas, initially out of equilibrium, to relax to the expected equilibrium state. Specifying the equilibrium (constant) value of density ρ and the initial temperature T_1 , the following equations are employed to determine the equilibrium atomic mass fraction α and the equilibrium temperature T :

$$\alpha^2/(1 - \alpha) = (m_m/4\rho) K_c \quad (16a)$$

and

$$T = \frac{2}{7 - \alpha} \left(\frac{5}{2} T_1 - \alpha \frac{E_a}{k} \right), \quad (16b)$$

where m_m is the molecular mass. It is assumed initially that the translational and rotational modes are in equilibrium, and that the gas is purely diatomic. For the values of $\rho = 3 \text{ kg m}^{-3}$ and $T_1 = 35\,640 \text{ K}$, it is found that $\alpha = 0.5$ and $T = 10\,000 \text{ K}$. The study of constant volume relaxation is employed to investigate different phenomena. First, it is necessary to ensure that the dissociation and recombination

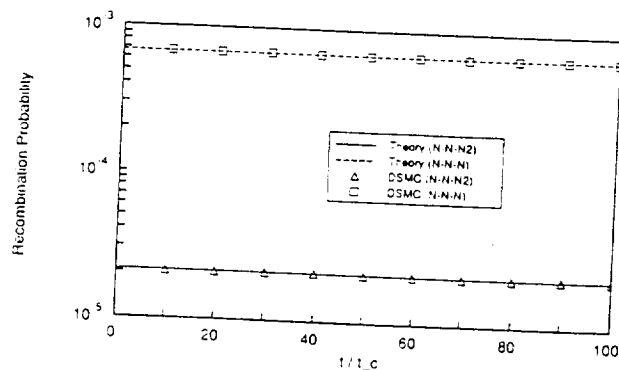


FIG. 2. Comparison of average recombination probabilities.

models lead to the correct equilibrium values predicted in Eqs. (16). Second, the effect of using different chemical rate coefficients is considered. The dissociation rates employed are those in Eqs. (15) and the following coefficients due to Kewley and Hornung:¹⁹

$$k_f(N_2 - N_2) = 3.82 \times 10^{-1} T^{-3.5} \times \exp\left(-\frac{113\,200}{T}\right) \text{ m}^3/\text{molecule}/\text{sec}, \quad (17a)$$

$$k_f(N_2 - N) = 1.41 \times 10^{-4} T^{-2.5} \times \exp\left(-\frac{113\,200}{T}\right) \text{ m}^3/\text{molecule}/\text{sec}. \quad (17b)$$

The temperature dependence of the rate coefficients in Eqs. (15) and (17) is significantly different. In these simulations, a value of $\phi = 0$ is employed in the dissociation model. Finally, to assess the importance of three-body reactions, the simulation is performed without recombination reactions.

The results of each of these investigations are given in Fig. 3, where the variation of α with time is shown. The solid curve represents the relaxation behavior using Byron's rate data. The chemistry models drive the mass fraction of atomic nitrogen to its expected equilibrium value. The dotted curve represents the simulation performed with the rate coefficients defined by Kewley. With these values the simulation, again, attains the equilibrium value, but the rise in α is significantly slower than for the computations that employed the coefficients of Byron. This aspect of the simulations will be given further consideration in the computations behind strong shock waves. The dashed curve in Fig. 3 shows the relaxation behavior when the recombination reactions are omitted. The value of α will continue to rise until the gas consists purely of the atomic species. The effect of the absence of the recombination reactions only becomes apparent after the creation of a significant atomic nitrogen population. Further results from these three simulations are given in Fig. 4, where the vibrational temperature is shown. With Byron's rate coefficients, the expected equilibrium temperature is attained after a small maximum in vibrational tem-

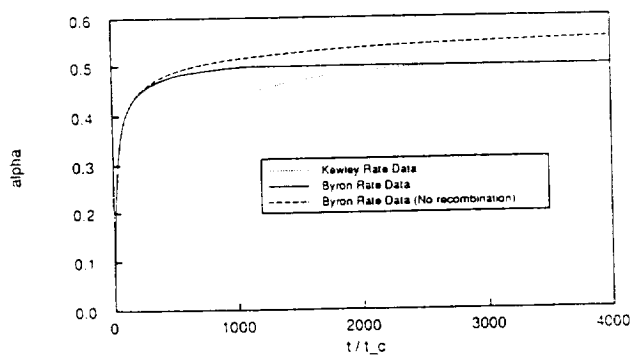


FIG. 3. Variation in time of the atomic mass fraction of a chemically relaxing gas.

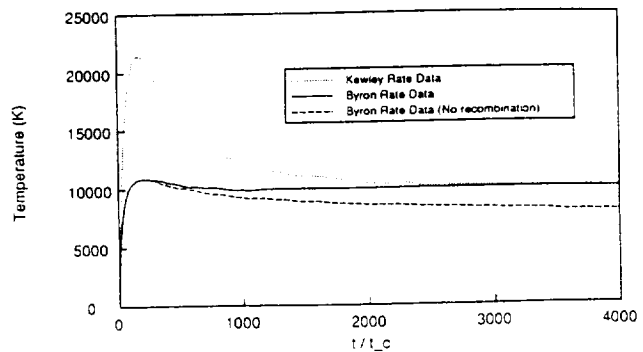


FIG. 4. Variation in time of the vibrational temperature of a chemically relaxing gas.

perature is reached. With Kewley's data, the peak vibrational temperature is much higher. This effect is due to the reduced rate of dissociation observed in Fig. 3. However, the vibrational temperature does finally reach the same steady-state value predicted in Eq. (16b). By failing to include the recombination reactions, it is observed that the temperature continues to decrease as dissociation continues unabated. The results in Figs. 3 and 4 serve to verify the chemistry models employed in the DSMC technique. The need for the inclusion of recombination in the simulation is demonstrated. The simulations also indicate that significant differences in flow properties may be computed with different rate coefficients.

Having verified the chemistry models under test conditions, they are now applied to the relaxation zone behind strong shock waves of nitrogen. Three different sets of conditions are considered and are listed in Table I. The subscript 1 indicates upstream conditions, subscript 2 indicates the point immediately after the shock that is in translational and rotational equilibrium, and no subscript indicates the downstream conditions. The flow parameters have been chosen to correspond to the conditions investigated experimentally by Kewley and Hornung,¹⁹ and computationally by Bird.⁵ In Fig. 5, the density profile is shown for case 1. The two sets of computations were performed first with the rate data of Kewley, then with the data of Byron. In each case, the vibration-dissociation coupling parameter ϕ was set to zero. This leads to a minimum of coupling between these phenomena. It is satisfying that the computations performed with Kewley's data does follow his experimental data. As may have been anticipated from Fig. 3, the computation that employed

TABLE I. Experimental conditions of shock waves investigated computationally.

Case	u_1 (km/sec)	ρ_1 (kg/m ³)	T_2 (K)	ρ/ρ_1
1	7.31	7.48×10^{-3}	25 013	14.9
2	5.60	2.86×10^{-2}	15 130	11.4
3	4.80	4.67×10^{-2}	11 405	10.0

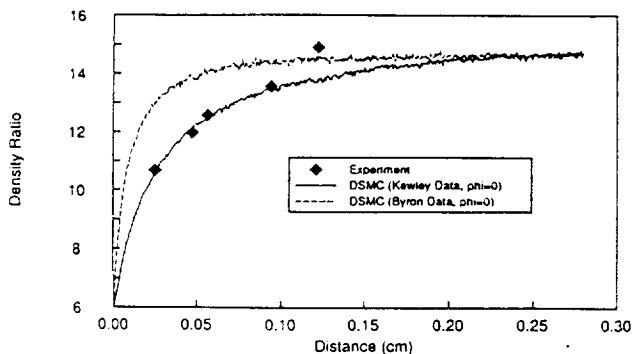


FIG. 5. Comparison of density profiles for case 1: computed with two different sets of rate coefficients and the same chemistry model.

Byron's data dissociates at an elevated rate in comparison with the experiment. The difference is primarily in the first few millimeters of the flow behind the shock.

The degree of vibrational nonequilibrium in the flow computed with Kewley's rate data is observed in Fig. 6, where the translational and vibrational temperatures are shown. For these flow conditions, the probabilities of vibrational energy exchange and dissociation just behind the shock are of the same order of magnitude. Hence, the coupling of the vibrational and dissociative processes is significant, and will limit the rate of reaction. Clearly, this phenomenon is most significant in the first few millimeters of the flow behind the shock. In the analysis performed by Kewley and Hornung to derive the rate coefficients, no coupling between vibration and dissociation was included. Hence the vibrational nonequilibrium behavior had to be included in the data by decreasing the temperature exponents and adjusting the leading constant. Alternatively, for Byron's experiments, the shock temperatures were significantly lower, so that the probability of vibrational energy exchange was several orders of magnitude higher than the dissociation probability. Under these conditions, the vibrational mode will be fully equilibrated prior to the onset of dissociation. Therefore it can be stated that the temperature dependence

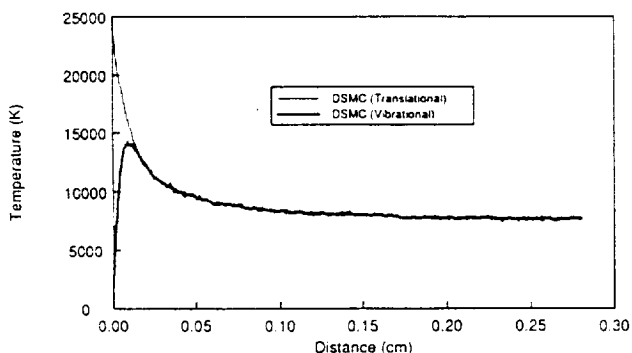


FIG. 6. Comparison of temperatures for case 1: computed with Kewley's rate data.

of the rate coefficients of Byron represents the behavior in vibrational equilibrium. Application of the equilibrium dissociation model [$\phi = 0$ in Eq. (4)] in the nonequilibrium flow therefore gives a rate of dissociation that is too high. There may, therefore, exist the possibility that the density profiles observed experimentally by Kewley and Hornung can be reproduced with Byron's equilibrium rate coefficients by applying an appropriate vibration-dissociation coupling model that will include the nonequilibrium effects immediately behind the shock.

One result of this approach is given in Fig. 7, where the density profiles behind the shock are again shown. By employing Byron's equilibrium rate data with the nonequilibrium model for nitrogen [$\phi = 3$ in Eq. (4)], it is found that the experimental data is very nearly reproduced. This encouraging result implies that rate data taken at moderate temperatures may be applicable at much higher temperatures, provided that an appropriate nonequilibrium model is employed. In Fig. 8, a comparison is shown of the vibrational temperatures computed using Kewley's data with $\phi = 0$, and Byron's data with $\phi = 3$. The computations with these rate coefficients were also performed for the experimental cases 2 and 3. The comparisons of density profile are shown in Figs. 9 and 10. Once again, it is found that the experimental data is reproduced with the combination of Byron's rate coefficients and the nonequilibrium vibration-dissociation coupled model.

Finally, the new models are applied to the flow conditions investigated spectroscopically by Sharma.²⁰ The flow was for nitrogen at an initial velocity and pressure of 6200 m/sec and 1 Torr at room temperature. The study provided rotational and vibrational temperatures at two different locations through the shock wave. The first was in the highly nonequilibrium region just after the shock front, and the second was further downstream in the equilibrium zone far behind the shock. For these conditions, the DSMC code was configured to compute the entire shock wave flow, commencing at the initial conditions. This differs from the other shock computations presented above which were begun at the point of translational-rotational equilibrium. In Fig. 11, the experimental measurements are compared with the pro-

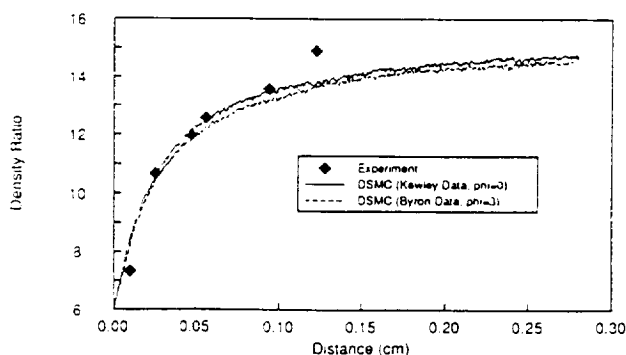


FIG. 7. Comparison of density profiles for case 1: computed with two different sets of rate coefficients and two different chemistry models.

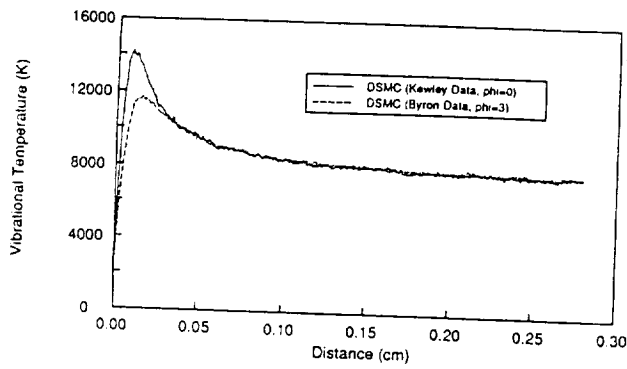


FIG. 8. Comparison of vibrational temperatures for case 1: computed with two different sets of rate coefficients and two different chemistry models.

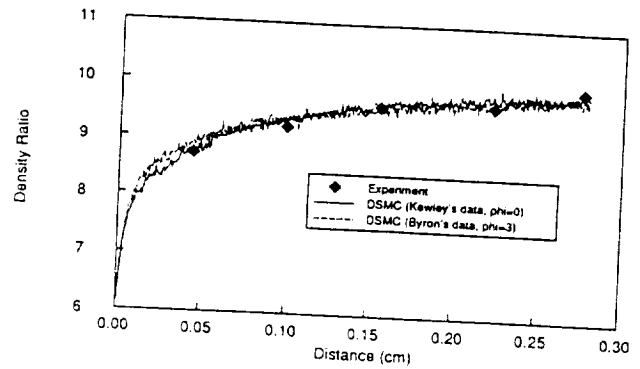


FIG. 10. Comparison of density profiles for case 3: computed with two different sets of rate coefficients and two different chemistry models.

files of rotational and vibrational (and translational) temperature computed with the DSMC technique. Good agreement is found between the numerical and experimental data. Near the shock front, the DSMC simulation reproduces quite well the separation in the rotational and vibrational temperatures. Further downstream, thermal equilibrium is attained with values close to the measured equilibrium condition. The small difference in the data in the downstream region of the flow may be attributed to the omission of ionized reactions, radiative cooling, and the presence of impurities in the experiment. The differences in the data in the nonequilibrium region must be resolved through further numerical and experimental studies. The computations were performed using the equilibrium rate data of Byron, together with the nonequilibrium vibration-dissociation-coupled model.

Each of the shock wave solutions presented in this study required about 4 h of CPU time on a Cray YMP supercomputer. In that time, over 3×10^9 collisions were computed for the 100 000 particles in the computational domain. Without a vectorized implementation of most of the DSMC algorithm, the computational cost would be increased by one order of magnitude on the supercomputer. Performing the computations on a modern workstation would increase the total computational time by a further factor of at least 5. While it can be argued that the use of such workstations is more cost effective (a supercomputer costs several million

dollars), it is proposed that a turnaround time of 200 h is undesirable for most researchers.

V. CONCLUSIONS

The relaxation zone behind several strong shock waves of nitrogen have been computed using the direct simulation Monte Carlo method, and excellent agreement was found with available experimental data. The intensive computational cost of the simulations was reduced dramatically through execution on a supercomputer of a vectorized implementation of the algorithm. For compatibility with the vectorized implementation, a new scheme for treating three-body recombination reactions was formulated. The model represents an improvement on previous recombination schemes, and reproduces the predicted results under test conditions. The most important aspect of the study relates to the interpretation of different sets of chemical rate coefficients. For shocks that exhibit significant vibrational nonequilibrium, the experimental density profiles may be computed successfully in two different ways. First, by employing an equilibrium dissociation model, which has no vibration-dissociation coupling, together with the rate data derived from the experiment assuming vibrational equilibration. Second, by employing a nonequilibrium, coupled vibration-

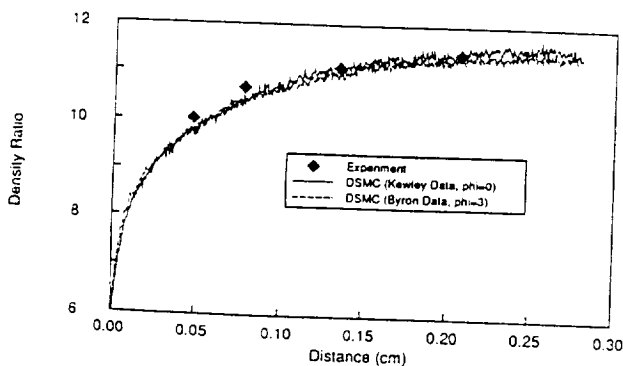


FIG. 9. Comparison of density profiles for case 2: computed with two different sets of rate coefficients and two different chemistry models.

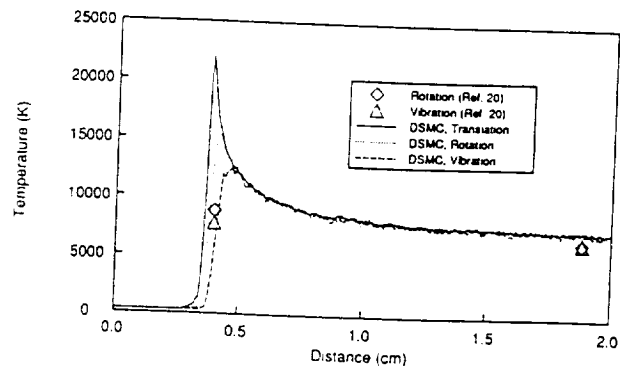


FIG. 11. Comparison of temperature profiles for the experiment of Sharma.

al-dissociation model, together with rate data taken in a separate investigation under equilibrium conditions. Clearly, the latter course of action is preferred, and is an important finding of the present investigation.

ACKNOWLEDGMENT

Support for the author was provided by NASA (Grant No. NCC2-582).

¹G. A. Bird, *Molecular Gas Dynamics* (Clarendon, Oxford, 1976).

²G. Pham-Van-Diep, D. Erwin, and E. P. Muntz, *Science* **245**, 624 (1989).

³I. D. Boyd, *Phys. Fluids A* **2**, 447 (1990).

⁴I. D. Boyd, *Phys. Fluids A* **3**, 1785 (1991).

⁵G. A. Bird, *J. Comput. Phys.* **25**, 353 (1977).

⁶I. D. Boyd, *J. Comput. Phys.* **96**, 411 (1991).

⁷D. Baganoff and J. D. McDonald, *Phys. Fluids A* **2**, 1248 (1990).

⁸G. A. Bird, *Progress in Astronautics and Aeronautics Series* (AIAA, Washington, D.C., 1989), Vol. 118, p. 211.

⁹I. D. Boyd, *AIAA J.* **28**, 1997 (1990).

¹⁰I. D. Boyd, *J. Thermophys.* **4**, 478 (1990).

¹¹R. C. Millikan and D. R. White, *J. Chem. Phys.* **39**, 3209 (1963).

¹²G. A. Bird, *Progress in Astronautics and Aeronautics Series* (AIAA, New York, 1981), Vol. 74, Part 1, p. 252.

¹³B. L. Haas and I. D. Boyd (in preparation, see also AIAA Paper No. 91-0774).

¹⁴C. Borgnakke and P. S. Larsen, *J. Comput. Phys.* **18**, 405 (1975).

¹⁵B. L. Haas, Ph.D. thesis, Stanford, 1990.

¹⁶F. E. Lumpkin, B. L. Haas, and I. D. Boyd, *Phys. Fluids A* **3**, 2282 (1991).

¹⁷W. G. Vincenti and C. H. Kruger, *Introduction to Physical Gas Dynamics* (Wiley, New York, 1965).

¹⁸S. Byron, *J. Chem. Phys.* **44**, 1378 (1966).

¹⁹D. J. Kewley and H. G. Hornung, *Chem. Phys. Lett.* **25**, 531 (1974).

²⁰S. P. Sharma, *Proceedings of 18th International Shock Tube Symposium* Tohoku, Japan, 1991, in press).

APPENDIX B

Evaluation of Thermochemical Models for
Particle and Continuum Simulations of Hypersonic Flow

Iain D. Boyd[†] and Tahir Gökçen[†]
Eloret Institute, 3788 Fabian Way
Palo Alto, California.

Abstract

Computations are presented for one-dimensional, strong shock waves that are typical of those that form in front of a reentering spacecraft. The fluid mechanics and thermochemistry are modeled using two different approaches. The first employs traditional continuum techniques in solving the Navier-Stokes equations. The second approach employs a particle simulation technique, the direct simulation Monte Carlo method (DSMC). The thermochemical models employed in these two techniques are quite different. The present investigation presents an evaluation of thermochemical models for nitrogen under hypersonic flow conditions. Four separate cases are considered that are dominated in turn by vibrational relaxation, weak dissociation, strong dissociation and weak ionization. In near-continuum, hypersonic flow, the nonequilibrium thermochemical models employed in continuum and particle simulations produce nearly identical solutions. Further, the two approaches are evaluated successfully against available experimental data for weakly and strongly dissociating flows.

Introduction

A space-vehicle passing through the earth's atmosphere will traverse a number of different flow regimes. At lower altitudes, the fluid density is sufficiently large for the flow to be considered in thermochemical equilibrium. However, as the vehicle ascends higher into the atmosphere, the molecular collision rate falls, and low-density effects become increasingly important.

[†] Research Scientist. Mailing address: NASA Ames Research Center, MS 230-2, CA 94035.

Continuum methods are successfully applied to flows in which the collision rate of the gas is sufficient to maintain Boltzmann energy distributions for the various thermal modes of the gas. It is not necessary that the temperatures associated with each of the different modes be equal, or that chemical equilibrium prevails. Particle methods, such as the direct simulation Monte Carlo method (DSMC), are successfully applied to flows in which a reduced collision rate no longer supports equilibrium energy distributions. As the numerical cost of this technique is proportional to the fluid density, application has mainly been limited to rarefied flows.

The computation of flow properties for the flight trajectories of many space vehicles require the use of both continuum and particle methods mentioned above. The interface between the different flow regimes is therefore of great importance. Clearly, it is desirable to obtain consistent results with these numerical methods in an overlapping near-continuum flow regime. Although the thermochemical models employed in continuum and particle methods are quite different, under conditions of thermochemical equilibrium they are expected to provide identical solutions. The relationship between the continuum and particle simulation under conditions of thermochemical nonequilibrium, however, has not been investigated thoroughly. It is therefore the purpose of the present paper to study this relationship by computing typical hypersonic flows with both the continuum and particle simulation methods.

Evaluation of the thermochemical models is made through the computation of four different cases. The flow conditions in the studies are given in Table 1 and are chosen to examine the effects of vibrational relaxation, dissociation, and ionization. These processes are considered in an accumulative sense through a gradual increase in the initial enthalpy of the flow. The continuum and particle approaches employed in this work are briefly described below.

Continuum Approach

In the continuum formulation, a nonequilibrium eleven species gas model for air (N_2 ,

$O_2, NO, N, O, N_2^+, O_2^+, NO^+, N^+, O^+, e^-$) has been implemented. The thermal state of the gas is described by three temperatures: translational, rotational and vibrational-electronic. The governing Navier-Stokes equations are supplemented by the equations accounting for thermochemical nonequilibrium processes. The equation set consists of fifteen partial differential equations: eleven mass conservation equations for species, one momentum equation for quasi one-dimensional flow, and three energy equations. Since the experimental data is for nitrogen gas, the subset (N_2, N, N_2^+, N^+, e^-) of the air model relevant to the dissociation and ionization of nitrogen is active. The thermochemistry model is basically that proposed by Park.¹⁻² The relaxation time for vibrational-translational energy exchange is taken from Millikan and White³ with Park's modification which accounts for the limiting cross-section at high temperatures. Another of Park's modifications concerning the diffusive nature of vibrational relaxation is not included, which is consistent with the current particle model. For vibration-dissociation coupling, the average vibrational energy lost or gained due to dissociation or recombination is taken as 30 percent of the dissociation energy.¹ The chemical reaction rates are prescribed by Park's model where the basic dissociation rate is assumed to be governed by the geometric average of translational and vibrational temperatures.

The numerical approach to solve the governing equations is fully implicit for fluid dynamics and chemistry. It uses flux vector splitting for convective fluxes, and shock capturing. An adaptive grid strategy is also implemented. For the computations in this paper, a quasi one-dimensional code is used and a freestream of pure nitrogen is prescribed. The details of the numerical method can be found in Refs. 4-6.

Particle Approach

The particle simulation code employed in this investigation provides modeling of the translational, rotational, vibrational, and electron kinetic energy distributions. These are complemented through simulation of dissociative, recombinative, ionizing, and exchange reactions. The code is vectorized for efficient execution on a Cray-YMP. Description of

the vectorized implementation can be found in Refs. 7 and 8. The boundary conditions employed in the one-dimensional flow are reflecting pistons set to the upstream and downstream velocities. The downstream velocity is obtained either from the continuum calculations, or from available experimental data. The present simulations compute the entire shock structure from upstream to downstream conditions. Once the shock reaches a specified location, small adjustments are made to the coordinate system of the computational grid to maintain a steady shock position.

The rate of energy exchange between the translational and rotational energy modes is simulated using a probability function evaluated using the energy of each collision.⁹ The mechanics of rotational energy exchange is performed by the Borgnakke-Larsen¹⁰ approach. The rate of energy exchange involving the vibrational energy mode is simulated using a high-temperature model.¹¹ The mechanics of vibrational energy exchange are computed using two different schemes. The first uses the Borgnakke-Larsen approach with a continuous vibrational energy distribution described by a fixed number of vibrational degrees of freedom, ζ_v . The second approach, due to McDonald,¹² allows sampling of post-collision vibrational energy levels from the discrete form of the Simple Harmonic Oscillator (SHO). This approach does not require the value of ζ_v to be estimated for the whole flowfield. Instead, it effectively varies ζ_v according to the local energy content of the flow, therefore it is the preferred approach from a physical standpoint. The manner in which the mechanics of energy exchange is performed in the particle simulation is shown by Lumpkin *et al.*¹³ to affect the rate of relaxation. Therefore, all the rotational and vibrational relaxation models employed in the particle simulations are adjusted to match the continuum values by the correction developed in Ref. 13.

Dissociation reactions are modeled with the Vibrationally Favored Dissociation model (VFD) proposed by Haas and Boyd.¹⁴ As its name suggests, this model includes the important physical phenomenon of vibration-dissociation coupling. The model contains a free parameter ϕ which controls the degree of coupling between vibrational and dissociative

relaxation processes. It was demonstrated in Ref. 14 that, by increasing the value of ϕ , it is possible to increase the dissociation incubation time in the simulation. Also in Ref. 14, through comparison with experimental data, the value of ϕ for nitrogen was determined assuming Borgnakke-Larsen mechanics for vibrational energy exchange with a fixed value for ζ_v . In the DSMC code, the model employed for the reverse recombination reaction appropriate to VFD is that developed by Boyd.⁸ All other chemical reactions, i.e., ionization and exchange reactions are simulated using the steric factor developed by Bird.¹⁵ The inclusion of electrons in the simulation is discussed in detail in Ref. 16.

Chemical Rate Coefficients

The rate coefficients employed in the reactions of interest in the present study are given in Table 2. These are described in the usual Arrhenius form:

$$k(T) = aT^b \exp(-E_a/kT)$$

where a and b are empirically determined constants, E_a is the activation energy, and T is the controlling temperature. Three different sets of coefficients are given corresponding to those used: in the continuum code; in previous DSMC investigations; and in the present DSMC code. The values of the activation energy used in the three sets of rate data are unchanged for each separate reaction. Therefore, the exponential term in the Arrhenius form has been omitted from Table 2.

The rate expressions employed in the continuum code are those recommended in the review by Park *et al.*² Generally, only the forward rate constants are specified. In the dissociation reactions, reactions 1 and 2, the controlling temperature in the continuum two-temperature approach is given by $T_a = (TT_v)^{1/2}$. For nitrogen dissociation, the particle code employs the rates of Byron¹⁷ in the Vibrationally Favored Dissociation model (VFD). It was shown previously by Boyd⁸ that these rates, when used with the VFD model, are capable of reproducing vibration-dissociation coupling observed at high temperatures.

The reverse rates for each reaction are obtained by evaluating the following temperature-

dependent form for the equilibrium constants proposed by Park:¹

$$\ln(K_e(T)) = A_1 z + A_2 + A_3 \ln(z) + A_4/z + A_5/z^2$$

where the A_i are constants and $z=10000/T$. In the continuum code, the values of A_i for reaction 3 are obtained from Ref. 18 while those for reaction 4 are taken from Ref. 1. Unfortunately, this form for the equilibrium constant is not mathematically convenient for implementation in the DSMC chemistry models. However, a set of reverse reaction rates for use in DSMC has been determined by Bird,¹⁹ and these have been used in a number of studies. These reverse reaction rates are determined by calculating an equilibrium constant in which the exponential terms in the electronic partition functions are evaluated at a temperature of 11,000 K. It is possible to compute the equilibrium constants employed by Bird by considering the ratio of the forward and reverse rates for each reaction. This has been performed for reactions 3 and 4 of Table 2. The equilibrium constant employed by Bird and that used in the continuum code are shown as a function of temperature for reaction 3 in Fig. 1. It should be noted that the exponential term has again been omitted for the sake of simplicity. For this reaction, it is found that the equilibrium constant employed by Bird is about 2 orders of magnitude higher than the continuum expression. In reaction 4, the equilibrium constant used by Bird gives values which are again generally higher than the continuum model.

It is to be noted that the goal of the present study is to evaluate differences in the chemical models employed in the continuum and particle methods. To limit the number of factors involved in our comparisons, it is the aim to maintain consistency between the relaxation rates employed in the solution techniques. Therefore, a form for the equilibrium constant which takes the traditional Arrhenius form is curve-fitted as a function of temperature to Park's expression. The limitation on the Arrhenius form which may be used conveniently in Bird's expression for the probability of chemical reaction¹⁵ is discussed by Boyd and Stark.²¹ The curve fit for reaction 3 is also shown in Fig. 1. The resulting rate constants for the reverse direction for reactions 3 and 4 are listed in Table 2. Gener-

ally, good agreement is obtained between the new DSMC expressions and Park's results, particularly over the temperature range of interest, i.e. from 5,000 to 20,000 K.

For reaction 5, the temperature dependent form proposed in Ref. 2 is not convenient for use in the DSMC chemistry models. In comparing the forward rate constants employed by Park and Bird for this reaction it is noted that Bird's reaction rates are several orders of magnitude lower. Once again, a curve fit is made to Park's expression in an Arrhenius form which may be employed in the particle chemistry models. The new form, which is given in Table 2, gives closer correspondence to Park's results over the temperature range of interest. Further analyses have been performed which improve the correspondence between the chemical rates employed in continuum and particle simulation for all reactions in air involving charged species and are reported in Ref. 16.

Presentation of Results

Computations are performed for four different sets of flow conditions for normal shock-waves in pure nitrogen and these are listed in Table 1 in which subscripts 1 and 2 indicate upstream and downstream conditions, respectively. The upstream temperature is prescribed to be 300 K for all cases. The upstream density together with the length of the computational domain simulated are chosen such that the flows are in the near-continuum regime. In other words, Knudsen number is small enough that the thickness of the shock wave is small compared to relaxation distance behind the shock. The different upstream flow conditions also provide increasing enthalpy: thus, the flow behind the shock is characterized in Case 1 by vibrational relaxation processes; in Case 2 by weak dissociation; in Case 3 by strong dissociation; and in Case 4 by weak ionization. The conditions in Cases 2 and 3 correspond to those investigated experimentally by Kewley and Hornung.²² The results for each of these investigations are described in the following sub-sections. The numerical parameters chosen for each DSMC computation followed the usual guidelines in setting the cell size less than the mean free-path and the time-step to be a fraction of the mean time between collisions. The cell size criterion is relaxed in regions far behind the

shock-front where flow gradients are less severe. In each case considered, the number of computational cells is 1,000 and the number of simulated particles is maintained at about 100,000.

Case 1: Vibrationally Relaxing Flow

Density profiles for the first case investigated are shown in Fig. 2. Very good agreement is found between the continuum and particle simulation results. Two different DSMC computations are shown: the first corresponds to the use of the Borgnakke-Larsen approach (BL) for performing the mechanics of vibrational energy exchange with a constant number of vibrational degrees of freedom, $\zeta_v=1.6$. This value corresponds closely to that evaluated at the downstream equilibrium temperature. The second solution employed the discrete vibrational energy sampling approach for the Simple Harmonic Oscillator (SHO) of McDonald⁷ which automatically varies ζ_v . This is the first time that a comprehensive comparison is made between continuum and particle simulations for vibrational relaxation behind a strong shock. It is very encouraging to observe that, under near-continuum conditions, the two methods give such close agreement.

The variation in translational and vibrational temperatures for this case are shown in Fig. 3. The particle solutions are obtained with McDonald's variable ζ_v model. Once again, very good agreement is obtained between the two solution techniques. Temperature is generally a much more sensitive quantity to simulate than density. The close correspondence between the continuum and particle results indicates that the vibrational relaxation models of both approaches are very nearly equivalent. This comparison therefore lends strong support to the use in the particle simulation of the vibrational energy exchange probabilities developed for the DSMC method,¹¹ the correction term required to equate the continuum and particle relaxation rates,¹³ and the mechanics of vibrational energy exchange.¹² It should be noted that the degree of dissociation under these flow conditions is less than 1%.

Case 2: Weakly Dissociating Flow

The second set of conditions considered has an increased enthalpy which gives rise to weak dissociation behind the shock. This case is of additional interest as it was studied experimentally by Kewley and Hornung²² who employed interferograms to measure the variation in density behind strong shocks of nitrogen. The increase in enthalpy is revealed in the density profiles shown in Fig. 4 in which the normalized density rise reaches a value of about 10 at the downstream boundary. While both solutions give good agreement with the experimental data, it is clear that the particle solution provides the better correspondence. The DSMC profile is obtained with the variable ζ_v model. Comparison of the translational and vibrational temperatures computed through the shock are shown in Fig. 5. Again, a very good agreement is observed for the two sets of results. Considering the excellent agreement obtained in Fig. 5 between the continuum and particle methods, and also for the case of vibrational relaxation, it is concluded that the differences observed in Fig. 4 must be due to the dissociation models employed in each simulation technique. This indicates that the continuum two-temperature model gives a dissociation rate which is slightly slower than that of experiment and DSMC. In other words, for a weakly dissociating gas, the effect of vibrational relaxation on dissociation is overestimated in Park's two-temperature model.

The results for the mole fractions of molecular and atomic nitrogen are shown in Fig. 6. As expected from the previous comparisons, there is close agreement between the two numerical approaches with DSMC predicting slightly more dissociation than is obtained in the continuum solution.

Case 3: Strongly Dissociating Flow

The further increase in enthalpy for Case 3 gives rise to stronger dissociation effects. Once again, the flow conditions modeled match those considered experimentally by Kewley and Hornung.²² The experimental profile of density behind the shock is compared with the computational results in Fig. 7. The comparison between the continuum solution and the experimental data is excellent. The DSMC profile is computed using the variable ζ_v

model and $\phi=2$. With this model configuration, the particle method provides excellent agreement with both the experiment and the continuum solution. It should be noted that this is the DSMC model configuration employed in the computations for Case 2.

The translational and vibrational temperature profiles computed with the continuum and DSMC techniques are shown in Fig. 8. Generally, very good agreement is observed between the two. There is a noticeable difference in the peak vibrational temperatures computed by the two methods. This has quite significant implications for the estimation of radiative emission in such flows. The difference is attributable to dissociation-vibration coupling, i.e., how the vibrational energy distribution is affected by dissociation. This process is modeled quite differently in the continuum and particle approaches. These results indicate the need for experimental measurement of vibrational temperature profiles behind shock waves under conditions similar to those considered here. For completeness, the profiles of mole fractions of the neutral species are shown in Fig. 9. The stronger degree of dissociation for these flow conditions is very evident and, as expected, very good agreement is found between the two solutions.

For this strongly dissociating case, it is found that Park's two temperature model reproduces the experimental data very well. It is very encouraging that the two temperature model gives such a favorable comparison with the experimental data in strongly dissociating flow as this is the regime for which the model has been developed. Indeed, the present comparison arguably provides the strongest evidence to date that, despite its weak theoretical basis, the two-temperature model does produce adequate simulation of strongly coupled vibration-dissociation processes. The present investigation is unique in that evaluation of the model is performed through direct comparison with experimental measurements of a fundamental flow quantity. The model was previously calibrated against experimental data by Park¹ through comparison with radiation emission spectra, and by Candler²³ through comparison with shock stand-off distance. Due to the excellent comparisons between DSMC and experiment in Figs. 4 and 7, it is recommended that Mc-

Donald's collision mechanics and the VFD model with $\phi=2$ be used for simulating nitrogen dissociation with the particle method.

Case 4: Weakly Ionizing Flow

The increase in enthalpy for Case 4 is sufficient to give rise to significant ionization effects behind the shock. In performing the DSMC computations of the ionized flowfield, a steady shock solution is first obtained with the ionizing reactions omitted. After reaching this point, the ionized species are included and a further short transient phase in the simulation then allowed before sampling of flow properties is commenced. These procedures are adopted because the inclusion of electrons in the flowfield requires a reduction in computational time-step by two orders of magnitude. To compute the entire flowfield with such a small time-step would require much larger computational resources. The comparison for density profiles computed with the numerical techniques is shown in Fig. 10. As with the previous cases, good agreement is obtained between the two solutions. The temperature profiles computed with the continuum and particle methods for the translational and vibrational modes are compared in Fig. 11. The peak values for each energy mode are in good agreement. It is observed that the translational temperature shock computed with DSMC is thicker than the continuum result. This is due to the relatively low upstream density employed in this investigation. A more thorough analysis of such behavior will form the basis of future study. The computed variations in mole fractions for the neutral species obtained with the numerical techniques are compared in Fig. 12 and those for the charged species are compared in Fig. 13. The agreement which is generally obtained is very satisfactory. This comparison verifies that the new forms of the reverse reaction rates employed in the particle simulation are nearly equivalent to the expressions used in the continuum analysis. It should be noted that a degree of statistical scatter is exhibited by the DSMC results for the less abundant species.

To assess the effect of using the new reaction rates, a particle simulation is also performed with the rate data used by Bird.¹⁹ The variation in the mole fractions of the

charged species computed in this way are compared with the continuum results in Fig. 14. None of the species profiles are found to be in good agreement. With Bird's rates, the most populous ion is N_2^+ , whereas the new particle rate data agrees with the continuum solution in giving N^+ as the most abundant ion. With Bird's rate data, the mole fraction of electrons at the downstream boundary is about 2.5×10^{-3} whereas the continuum simulation gives a value of about 1.8×10^{-2} . If it is accepted that the rate coefficients provided in Refs. 1 and 2 are the more physically realistic, these large differences observed with Bird's older data set must call into question previous DSMC investigations which employed those reaction rates. Apparently, there has been a mistake in the reverse rate for reaction 3 used by Bird.¹⁹ The temperature exponent should be listed as -0.18 instead of the value of -0.52.²⁰ This error is quite serious as it was included in codes employed in a fairly large number of studies.

Concluding Remarks

This study was motivated by the requirement to evaluate the relationship between continuum and particle simulations of hypersonic flows in the near-continuum regime. The results obtained in the investigation have established that a close correspondence exists between the thermochemical nonequilibrium models employed in these solution techniques. In the case of vibrational nonequilibrium, the agreement between the two sets of numerical results validated a number of recent modeling developments for computing the rate and mechanics of vibrational energy exchange in the particle simulation. In the cases of weak and strong dissociation, both the continuum and particle models for vibration-dissociation coupling were successfully evaluated against experimental data. This is a most interesting result considering the large differences in the dissociation models employed in the two techniques. In the case of weakly ionized flow, it was necessary to develop new forms for some of the chemical rate constants for use in the particle simulation. These were developed so as to be nearly consistent with the continuum expressions, and also to be mathematically convenient for use in the particle chemistry models. The next stage in this continuing investigation will be evaluation of these methods for flow conditions in the

transition regime, i.e. at higher Knudsen numbers. In such flows, rarefaction effects may invalidate use of the Navier-Stokes equations, and give rise to large differences between the continuum and particle simulation results.

Acknowledgements

Support by NASA for I.D.B. (Grant NCC2-582) and for T.G. (Grant NCC2-420) is gratefully acknowledged.

References

- ¹ Park, C., *Nonequilibrium Hypersonic Aerothermodynamics*, John Wiley and Sons, Inc., New York, 1989.
- ² Park, C., Howe, J.T., Jaffe, R.L., and Candler, G.V., "Chemical-Kinetic Problems of Future NASA Missions," AIAA Paper 91-0464, January 1991.
- ³ Millikan, R. C., and White, D. R., "Systematics of Vibrational Relaxation," *Journal of Chemical Physics*, Vol. 39, No. 12, 1963, pp. 3209-3213.
- ⁴ MacCormack, R. W., "Current Status of the Numerical Solutions of the Navier-Stokes Equations," AIAA paper 85-0032, January 1985.
- ⁵ Candler, G.V., "The Computation of Weakly Ionized Hypersonic Flows in Thermo-Chemical Nonequilibrium," *Ph. D. Thesis*, Stanford University, 1988.
- ⁶ Gökçen, T., "Computation of Hypersonic Low Density Flows with Thermochemical Nonequilibrium," *Ph. D Thesis*, Stanford University, 1989.
- ⁷ Boyd, I.D., "Vectorization of a Monte Carlo Method For Nonequilibrium Gas Dynamics," *Journal of Computational Physics*, Vol. 96, 1991, pp. 411-427.
- ⁸ Boyd, I.D., "Analysis of Vibration-Dissociation-Recombination Processes Behind Strong Shock Waves of Nitrogen," *Physics of Fluids A*, Vol. 4, No. 1, 1992, pp. 178-185.
- ⁹ Boyd, I.D., "Analysis of Rotational Nonequilibrium in Standing Shock Waves of Nitrogen," *AIAA Journal*, Vol. 28, No. 11, 1990, pp. 1997-1999.
- ¹⁰ Borgnakke, C. and Larsen, P.S., "Statistical Collision Model for Monte Carlo Simulation of Polyatomic Gas Mixtures," *Journal of Computational Physics*, Vol. 18, 1975, pp. 405-420.
- ¹¹ Boyd, I.D., "Rotational and Vibrational Nonequilibrium Effects in Rarefied Hypersonic Flow," *Journal of Thermophysics and Heat Transfer*, Vol. 4, No. 4, 1990, pp. 478-484.
- ¹² McDonald, J.D., "A Computationally Efficient Particle Simulation Method Suited to Vector Computer Architectures," *Ph. D. Thesis*, Stanford University, 1990.

- ¹³ Lumpkin, F.E., Haas, B.L., and Boyd, I.D., "Resolution of Differences Between Collision Number Definitions in Particle and Continuum Simulations," *Physics of Fluids A*, Vol. 3, No. 9, 1991, pp. 2282-2284.
- ¹⁴ Haas, B.L. and Boyd, I.D., "Models for Vibrationally-Favored Dissociation Applicable to a Particle Simulation," AIAA Paper 91-0774, January 1991.
- ¹⁵ Bird, G.A., "Simulation of Multi-dimensional and Chemically Reacting Flows," in *Rarefied Gas Dynamics*, edited by R. Campargue, CEA, Paris, 1979, pp. 365-388.
- ¹⁶ Boyd, I.D. and Whiting, E.E., "Decoupled Predictions of Radiative Heating in Air Using a Particle Simulation Method," AIAA Paper 92-2971, July 1992.
- ¹⁷ Byron, S., "Shock-Tube Measurement of the Rate of Dissociation of Nitrogen," *Journal of Chemical Physics*, Vol. 44, Feb. 1966, pp. 1378-1388.
- ¹⁸ Mitcheltree, R.A., "A Parametric Study of Dissociation and Ionization at 12 km/sec," AIAA Paper 91-1368, June 1991.
- ¹⁹ Bird, G.A., "Nonequilibrium Radiation During Re-entry at 10 km/s," AIAA Paper 87-1543, June 1987.
- ²⁰ Bird, G.A., private communication, Killara, Australia, July 1992.
- ²¹ Boyd, I.D. and Stark, J.P.W., "Direct Simulation of Chemical Reactions," *Journal of Thermophysics and Heat Transfer*, Vol. 4 (3), 1990, pp. 391-393.
- ²² Kewley, D.J. and Hornung, H.G., "Free-Piston Shock-Tube Study of Nitrogen Dissociation," *Chemical Physics Letters*, Vol. 25, No. 4, 1974, pp. 531-536.
- ²³ Candler, G.V., "On the Computation of Shock Shapes in Nonequilibrium Hypersonic Flows," AIAA Paper 89-0312, January 1989.

Table 1. Flow conditions.

Case	U_1 (m/s)	ρ_1 (kg/m ³)	p_1 (torr)	U_2 (m/s)
1	4000	1.75×10^{-3}	1.17	541
2	4800	4.67×10^{-2}	31.2	480
3	7310	7.48×10^{-3}	5.00	496
4	10000	5.00×10^{-4}	0.33	640

Table 2. Leading constants in chemical rate data ($\text{m}^3/\text{molecule/s}$).

	Reaction	Continuum ²	Particle ¹⁹	Particle (present)
1.	$\text{N}_2 + \text{N}_2 \rightarrow 2\text{N} + \text{N}_2$	$1.16 \times 10^{-8} \text{ T}^{-1.6}$	$6.17 \times 10^{-9} \text{ T}^{-1.6}$	$7.97 \times 10^{-13} \text{ T}^{-0.5}$
2.	$\text{N}_2 + \text{N} \rightarrow 2\text{N} + \text{N}$	$4.98 \times 10^{-8} \text{ T}^{-1.6}$	$1.85 \times 10^{-8} \text{ T}^{-1.6}$	$7.14 \times 10^{-8} \text{ T}^{-1.5}$
3a.	$\text{N}^+ + \text{N}_2 \rightarrow \text{N} + \text{N}_2^+$	$1.66 \times 10^{-18} \text{ T}^{0.5}$	$1.67 \times 10^{-17} \text{ T}^{-0.18}$	$1.66 \times 10^{-18} \text{ T}^{0.5}$
3b.	$\text{N} + \text{N}_2^+ \rightarrow \text{N}^+ + \text{N}_2$	See Ref. 1	$2.37 \times 10^{-18} \text{ T}^{-0.52}$	$2.34 \times 10^{-14} \text{ T}^{-0.61}$
4a.	$\text{N} + \text{N} \rightarrow \text{N}_2^+ + \text{e}^-$	$7.31 \times 10^{-23} \text{ T}^{1.5}$	$2.98 \times 10^{-20} \text{ T}^{0.77}$	$7.31 \times 10^{-23} \text{ T}^{1.5}$
4b.	$\text{N}_2^+ + \text{e}^- \rightarrow \text{N} + \text{N}$	See Ref. 1	$8.88 \times 10^{-10} \text{ T}^{-1.23}$	$1.57 \times 10^{-17} \text{ T}^{0.85}$
5.	$\text{N} + \text{e}^- \rightarrow \text{N}^+ + 2\text{e}^-$	$4.15 \times 10^4 \text{ T}^{-3.82}$	1.00×10^{-14}	$5.81 \times 10^{-8} \text{ T}^{-1.0}$

chemical rate data.

MISSING
PRECEDING PAGE ~~BLANK~~ NOT FILMED

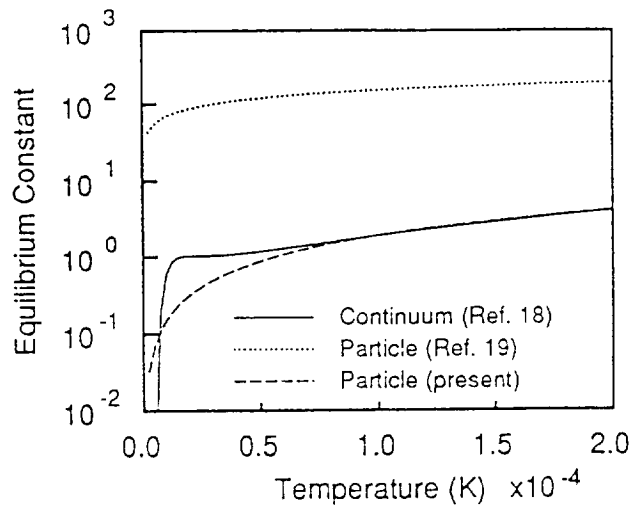


Fig. 1. Boyd & Gökçen

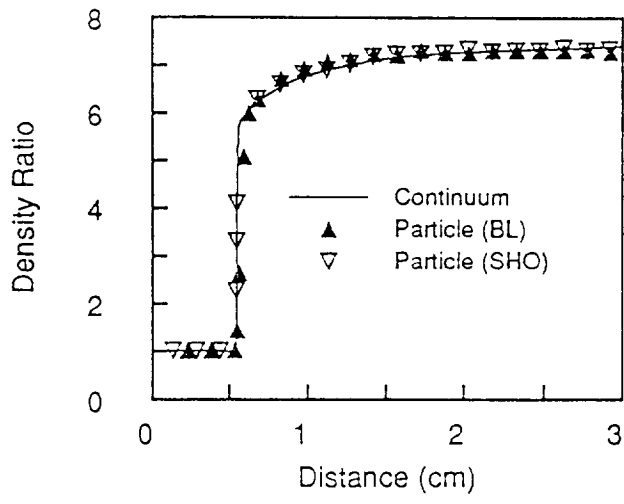


Fig. 2. Boyd & Gökse

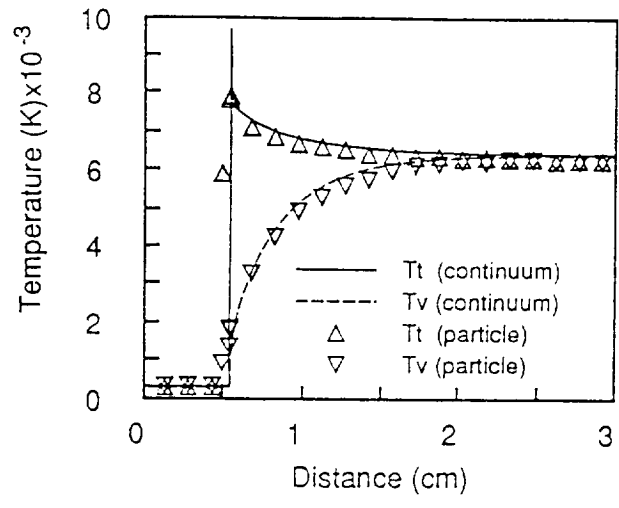


Fig. 3. Boyd & Gökçen

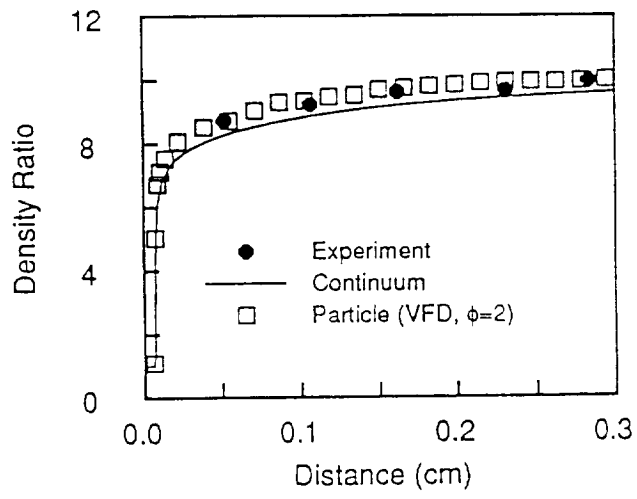


Fig. 4. Boyd & Gökçen

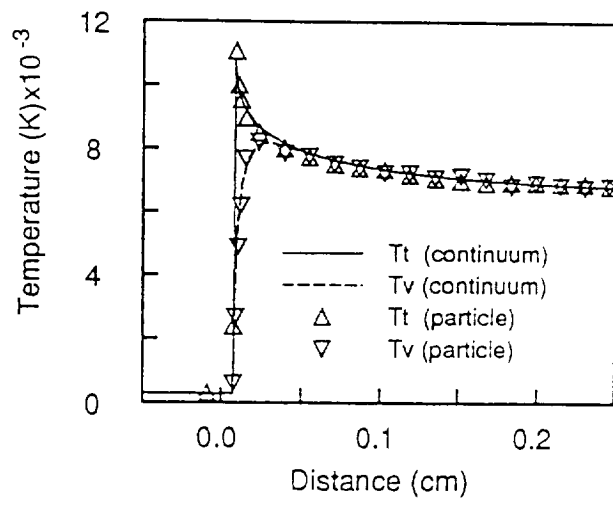


Fig. 5. Bayd & Gökçen

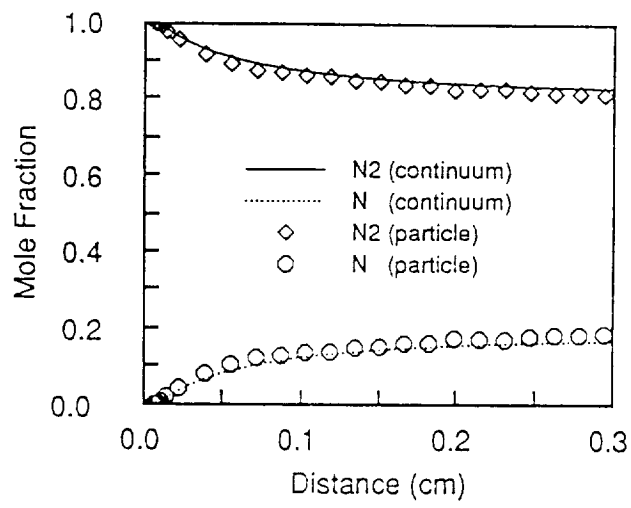


Fig. 6. Boyd & Gökçen

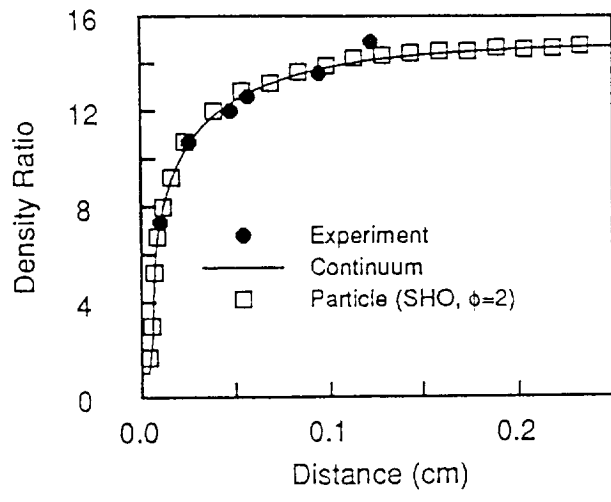


Fig. 7. Bad & Göksen

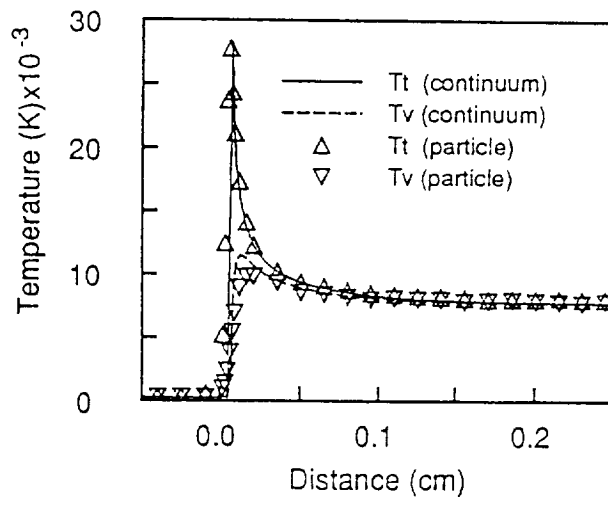


Fig. 8. Boyd & Gökçen

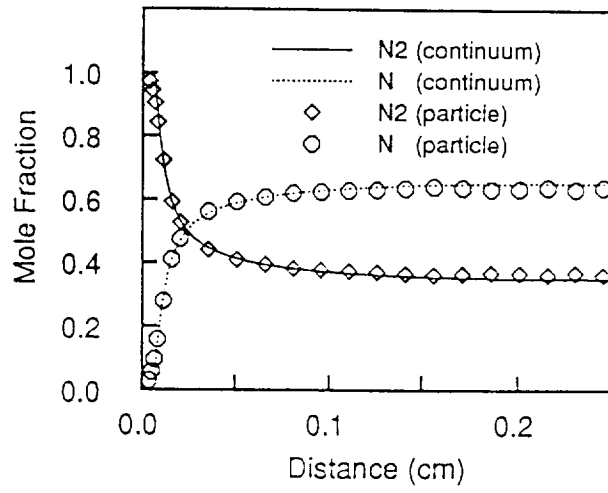


Fig. 9. Boyd & Gökçen

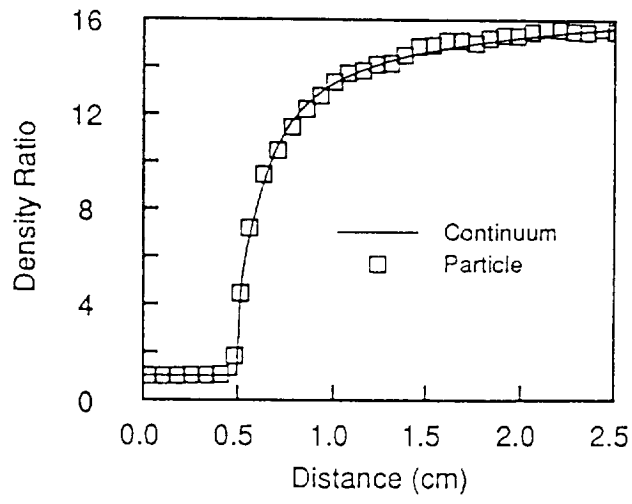


Fig. 10. Boyd & Gökse

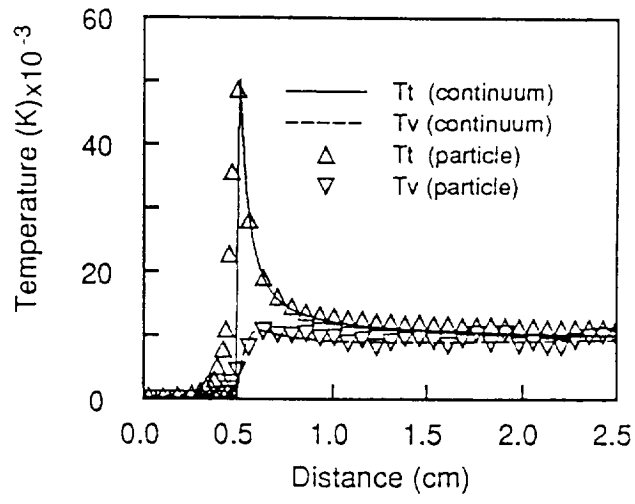


Fig. 11. Boyd & Gohsen

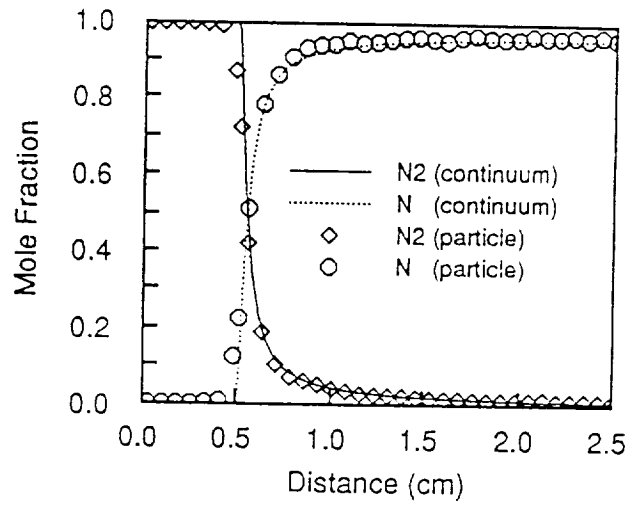


Fig. 12. Boyd & Götsen

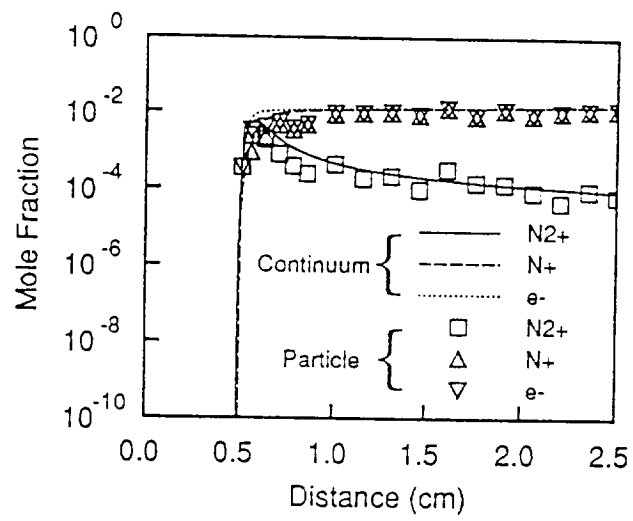


Fig. 13. Boyd & Götzen

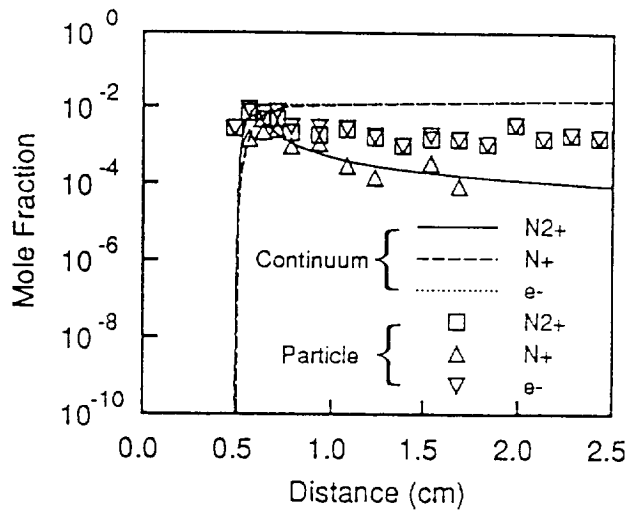


Fig. 14. Boyd & Götz

APPENDIX C



AIAA-92-2971

**Decoupled Predictions of
Radiative Heating in Air
Using a Particle Simulation Method**

I. D. Boyd and E. E. Whiting

Eloret Institute

Palo Alto, CA 94303.

**AIAA 23rd
Plasmadynamics & Lasers Conference
July 6-8, 1992 / Nashville, TN**

DECOUPLED PREDICTIONS OF RADIATIVE HEATING IN AIR USING A PARTICLE SIMULATION METHOD

Iain D. Boyd* and Ellis E. Whiting*

Eloret Institute, 3788 Fabian Way
Palo Alto, California.

Abstract

The radiative emission along the stagnation streamline and the radiative heating at the stagnation point of a blunt-nosed vehicle entering the Earth's atmosphere at hypersonic speed are estimated using a particle simulation technique with decoupled radiation. The fluid mechanics of the weakly ionized flow is computed using the direct simulation Monte Carlo method, DSMC. Analysis of radiation is decoupled from the flowfield and is estimated using NEQAIR, a computer code written by Park. The results are compared with previous DSMC computations which employed a simplified, coupled radiation model. The effects of recent advances in modeling relaxation and dissociative behavior with the DSMC technique are assessed in terms of radiative emission. It is found that the introduction of the new models decreases the predicted total radiative heating at the stagnation point of the vehicle by a factor of 15. The DSMC approach is also compared with a continuum flow model: in each case prediction of radiation is decoupled from the flowfield. Similar sets of vibrational and chemical relaxation rates are employed in these simulations. Despite large differences in the computed flowfield, which exhibits strong thermo-chemical nonequilibrium, the total predicted radiative heating estimates agree within a factor of 2.

Introduction

The motivation for the present study arises from the requirement for accurate radiation estimates for hypersonic flight vehicles. These are necessary for adequate thermal protection of the spacecraft during entry into the Earth's atmosphere. A previous study for the Aeroassist Flight Experiment (AFE) has been re-

ported by Whiting and Park¹ in which flowfield data were obtained using the Navier-Stokes equations at the lower altitudes traversed by the AFE during its sweep through the upper atmosphere. However, at higher altitudes, numerical difficulties were found in obtaining solutions. These difficulties are presumed to arise from the failure of the Navier-Stokes equations when the Knudsen number of the flow is too high.

The primary aim of the present study is to obtain radiation estimates using a particle simulation method for low-density, hypersonic flows in which strong effects due to thermo-chemical nonequilibrium are present and to compare the results with those from Ref. 1 for continuum flow. This is accomplished using the direct simulation Monte Carlo method (DSMC) to predict the one-dimensional flowfield along the stagnation streamline. The radiative emission is then computed using the computer code NEQAIR² with the radiation decoupled from the flowfield solution.

This is the first time that radiative heating has been estimated from DSMC computations using the approach in which radiation is decoupled from the flowfield solution. A new particle simulation code has been developed for the study. The code contains many recent developments which have improved considerably the modeling of thermo-chemical relaxation with the DSMC technique.

The new code is first evaluated through comparison against previously published particle computations of hypersonic, low-density, radiating flow. These previous DSMC computations employed simplistic thermo-chemistry models, and the effect of the introduction of the improved models is assessed. Additionally, comparison is made between the new code and continuum techniques for flow conditions corresponding to a trajectory point of the AFE vehicle. The continuum code

* Research Scientist. Mailing address:

NASA Ames Research Center, MS 230-2, CA 94035.

This paper is declared a work of the U.S. Government and is not subject to copyright protection in the United States.

is SPRAP (Stagnation Point Radiation Program) written by Park³ which solves the Navier-Stokes equations. Radiative emission for these continuum calculations is also decoupled from the flowfield solution.

Description of the Particle Simulation

The particle simulation code for computing one-dimensional shock waves in air is highly vectorized, and has been extended from the implementation for a reacting gas described by Boyd⁴ to include electrons and ionizing reactions. An eleven species (N_2 , N , O_2 , O , NO , N_2^+ , N^+ , O_2^+ , O^+ , NO^+ , E^-) real air model is employed. The code contains many recent modeling developments which have improved the ability of the DSMC technique to simulate thermochemical relaxation phenomena.

The code simulates rotational⁵ and vibrational⁶ energy exchange using probability functions which are evaluated using the energy of each collision. These represent an improvement on previous models in which constant probabilities were applied. The code employs the Vibrationally-Favored Dissociation model of Haas and Boyd⁷ and a corresponding recombination model.⁴ From the DSMC simulation, it is assumed that the vibrational and electronic temperatures of the gas are equal for the purposes of computing the radiative emission. Therefore, it is expected that the improved physical models employed in the DSMC code may affect significantly the total radiative heating predicted.

The introduction of electrons into the code requires special consideration. Due to their very low mass, the collision rates associated with electrons are about two orders of magnitude higher than those associated with the heavy species which occur in air. This requires the use of a numerical time-step which is two orders of magnitude smaller than would be employed were the electrons absent from the flowfield. In the present implementation, this problem is solved by using a time-step based on the heavy species to move the particles through the flowfield, and then subdividing the time-step into one hundred sub-steps to perform the collisions. Charge-neutrality is enforced throughout the flowfield by forcing each electron to remain in the same computational cell as the ion with which it was initially formed. While this is physically unrealistic, this approach should not affect the prediction of radiative emission to any great extent. Also,

any charged particles which collide with the cold surface of the vehicle are assumed to recombine to the neutral species. The special considerations described here for simulating charged species add a significant numerical overhead to the calculations (although the DSMC code is still highly vectorized). This overhead is minimized by initially running the DSMC code without the charged species until a steady state is reached. The ionization and charge-exchange reactions are then turned on, and the system is allowed to reach a new steady state, before sampling of flow variables begins.

Two different sets of chemical rate data are employed in the DSMC code. The first corresponds to that used by Moss *et al.*⁸ This set was implemented without coupled vibration-dissociation. In addition, for each reaction, the reverse rate expressions were determined by evaluating the electronic partition functions in the equilibrium constants at a fixed temperature. The second set of rate constants is based on those employed by Whiting and Park in the continuum code SPRAP. In their analysis, the reverse reaction rates are obtained by evaluating temperature-dependent curve fits for the equilibrium constant. The curve fits take the following form proposed by Park³:

$$K_e(T) = \exp(A_1 + A_2 \ln(z) + A_3 z + A_4 z^2 + A_5 z^3)$$

where the A_i are constants and $z=10000/T$. Unfortunately, this form for the equilibrium constant is not mathematically convenient for implementation in the DSMC chemistry models.

The goal of this part of the present study is to evaluate differences in the chemical models employed in the continuum and particle methods. To limit the number of factors involved in these comparisons, it is the aim to maintain consistency between the relaxation rates employed in the solution techniques. Therefore, a form for the equilibrium constant which takes the traditional Arrhenius form is fit as a function of temperature to Park's expression. This approach has been very successfully applied by Boyd and Gökçen⁹ to the ionizing reactions for N_2 . By achieving good correspondence between the two sets of chemical rate constants, very good agreement was obtained for flow solutions to hypersonic shock-waves in N_2 using particle and continuum methods. For air, good agreement is generally obtained between the new DSMC expres-

sions and Park's results over the temperature range of interest, i.e. from 10,000 to 20,000 K.

Description of NEQAIR

The code employed to estimate the radiative emission from the flowfield solution is called NEQAIR and was developed originally by Park.² NEQAIR calculates the nonequilibrium electronic excitation of the species in the flow and the radiation emitted by those species. A principal assumption made in the code is that the quasi-steady state (QSS) model may be used to determine the population of each electronic state of a species after the species density is found from the reacting-flow solution.

The QSS model assumes that the individual rates of populating and depopulating each electronic state are much faster than the rate of change of the population of the state itself. Thus, the population of a state is given by the difference of two large numbers that are about equal. This assumption is not valid in the flow immediately behind the shock wave where the populations of the excited states are low and increasing rapidly. However, as the excited states become populated, the species begin to emit radiation, and by the time the radiation reaches a significant level, the assumption is reasonably valid.

As the QSS model is applied after the chemistry portion of the calculation is completed, the electronic excitation processes are assumed to be independent of the chemical reactions. This simplifies the calculation enormously. The QSS model allows a separate effective electronic temperature to be defined for each excited electronic state. These temperatures are defined by comparing the population of an excited state to the population of the ground state. At each flowfield data point, the QSS model implemented in NEQAIR employs the translational and vibrational temperatures from the DSMC or continuum simulation. In addition, the QSS model assigns many temperatures for electronic excitation (one for each excited electronic state of every species).

In the estimation of radiative emission from the flowfield solution, NEQAIR is executed over 12 different spectral regions which are listed in Table 2. These have been determined by Whiting and Park¹ to be those which make significant contributions to the total radiative heating for hypersonic flows of air. The fol-

lowing molecular bands have been included: N_2^+ (1-), N_2 (1+), N_2 (2+), N_2 (BH1), $NO\beta$, $NO\gamma$, O_2 (SR).

The ultimate test of such codes is how well the results compare with experiment. Park¹⁰ has compared calculated radiative results with shock-tube, ballistic-range, and Earth-entry data covering a wide range of flight conditions and finds good agreement, generally within a factor of two.

Results and Discussion

This section is divided into three sub-sections. In the first, comparison is made between the new code and DSMC computations reported previously by Moss *et al.*⁸ A number of different comparisons are made to examine the ability of the new code to reproduce exactly the results of Ref. 8 using the same physical model and chemical reaction rates. Specifically, the DSMC code employs constant rotational and vibrational collision numbers of 5 and 50, and the chemical reaction rates from Ref. 8 with the degree of vibration-dissociation coupling set to zero. The second subsection investigates the effects of employing the improved physical models. For this purpose, the DSMC code employs variable rotational and vibrational collision numbers, vibrationally-favored dissociation, and the new chemical rate constants derived from the continuum expressions. In the third sub-section, comparison is made between the DSMC code using the new models and the continuum computations of Ref. 1.

Comparison with Previous Results Using Old DSMC Models

The new code is first assessed through comparison with DSMC computations presented by Moss *et al.*⁸ for the AFE at an altitude of 78 km (the flow conditions are given in Table 1). The free-stream temperature and Knudsen number were 188 K and 1.2×10^{-3} respectively. For compatibility with the study reported in Ref. 8, constant rotational and vibrational collision numbers of 5 and 50 are employed. Also, the chemical reaction rates from Ref. 8 are used, the degree of vibration-dissociation coupling is set to zero, and the shock standoff distance is specified as 0.110 m from the body. A total of 1,000 computational cells and over 100,000 simulated particles are employed in each of the calculations reported in the current work.

The temperatures computed in the present study

(lines) are compared with data taken from Ref. 8 (symbols) in Fig. 1. It is clear that significant thermal nonequilibrium effects are present. In comparison to the profiles from Ref. 8, the present temperatures are slightly higher. This effect is at least partially due to the absence of radiative cooling in the current work.

The mole fractions of the major species computed in the present study (lines) are compared with data taken from Ref. 8 (symbols) in Fig. 2. The present study is in very good agreement with the solutions from Ref. 8. In addition to the general form of the computed profiles shown in Figs. 1 and 2, the peak electron temperature of about 18,000 K and the maximum electron mole fraction of about 0.013 are in good correspondence to the results of Ref. 8.

The radiative emission along the stagnation streamline given by NEQAIR for the present DSMC flowfield solution is shown in Fig. 3. This profile compares quite well with the profile given in Ref. 8, although the peak value is somewhat larger in the present study. Integration of the spontaneous emission along the streamline to the body gives a one-dimensional radiative flux of $64.8 \text{ kW/m}^2/\text{sr}$, which is about a factor of 1.6 greater than the result of Moss *et al.* The difference may partly be accounted for in terms of radiative cooling which is omitted in the present calculations by estimating radiative emission decoupled from the flowfield. Considering the significant differences in the radiation models employed in the two studies, the agreement is acceptable.

The radiative heating at the stagnation point due to the radiative flux given above is found using a spherical cap model¹. First, the infinite slab result is obtained for the total radiative heating flux at the stagnation point by multiplying the one-dimensional value by 2π for the optically thin gas part of the spectrum, and by π for the self-absorbing regions. The spherical cap result is then computed as about 80% of the infinite slab value¹. This procedure gives a total radiative heating value of about 340 kW/m^2 , which is a very high value. This value is even higher than the convective heating rate reported in Ref. 8 as 248 kW/m^2 .

The contributions to the total radiative heating made by the various spectral regions which are analyzed are listed in Table 3 under Old Model. The reasonable agreement found between the present DSMC

results and those obtained in Ref. 8 for the radiative flux, indicates that the decoupled approach to radiation assumed in this study is an appropriate solution method for these flow conditions. In addition, analysis of the rate of loss of energy from the flowfield showed that only about 0.2% was due to radiative emission. This confirms that simulation of radiation coupled to the fluid mechanics is unnecessary for these flowfields.

Comparison of Old and New DSMC models

Having established that the new DSMC code provides solutions which are similar to previous studies, when using similar models, it is appropriate to assess the effect on the radiative emission by the introduction of the improved physical models. Specifically, variable rotational and vibrational collision numbers, vibrationally-favored dissociation, and the new chemical rate constants derived from the continuum expressions are implemented. The translational and vibrational temperatures computed with the DSMC code using the old and new models are shown in Fig. 4 for the same conditions considered in the previous subsection. The relaxation zone is much larger with the improved models. Note that the vibrational mode using the new model does not equilibrate with the translational mode until the body surface is reached. This is due mainly to the use of the variable vibrational collision number. This quantity is a strong function of temperature, and only reaches a maximum of about 50 at the peak translational temperature. For most of the stagnation streamline, the vibrational collision number is greater than 100 which reduces significantly the rate of equilibration of the vibrational mode.

The species which radiate most energy in the ultraviolet region of the spectrum ($0.11\text{-}0.18 \mu\text{m}$) are atomic nitrogen and oxygen. The variation in the mole fractions for these species is shown in Fig. 5. With the new, improved models, the rise in N and O due to dissociation is retarded significantly due to the use of the vibrationally-favored dissociation models and the lower vibrational temperatures. The strongest radiator above $0.2 \mu\text{m}$ is N_2^+ and its variation in mole fraction computed with the old and new DSMC models is compared in Fig. 6. The rise in N_2^+ is faster with the old models although behind the shock the two solutions show general agreement.

The profiles of radiative emission are compared in

Fig. 7. The peak emission obtained with the new models is significantly lower than that computed with the previous models due to the lower electronic temperature, which is set equal to the vibrational value in NEQAIR. The computed three-dimensional integrated radiative heating at the stagnation point is only about 23.4 kW/m^2 for the new model which is a factor of about 15 smaller than that predicted by the old model. The contributions to the total radiative heating made by the various spectral regions which are analyzed using NEQAIR are listed in Table 3 under New Model. The very large difference obtained in the radiative heating estimates using the old and new thermochemistry models demonstrates the sensitivity of the calculations to the physical models.

Comparison with Continuum Results

The DSMC code using the new models is applied to the flow conditions examined by Whiting and Park¹, which are given in Table 1. These are slightly different from those investigated in Ref. 8. The most important difference involves the shock standoff distance which is significantly larger in Ref. 1 (0.188 m) than in Ref. 8 (0.110 m). The freestream temperature is 188 K and the Knudsen number is 1.7×10^{-3} . The DSMC computations again employed the energy-dependent probabilities of rotational and vibrational energy exchange, and the vibrationally-favored dissociation model discussed by Boyd.⁴ The vibrational and chemical rate constants are made consistent with those employed in the continuum simulation as discussed earlier.

The continuum results taken from Ref. 1 were computed using SPRAP which was developed by Park.³ This code computes the viscous, one-dimensional, continuum flow behind an infinitely thin normal shock wave using the approach described in Ref. 3. The solution for the one-dimensional, uniform area duct may then be transformed to represent the flow along the stagnation streamline of a spherical body. The initial flow conditions immediately behind the shock are determined from the Rankine-Hugoniot shock-jump relationships, assuming that the vibrational temperature remains at the free-stream value. A viscous shock layer treatment is applied for computation of the boundary layer which forms next to the cold wall of the vehicle. It is assumed that the flow in the boundary layer is chemically frozen with a ratio of specific heats equal

to 11/9. Further, the wall is assumed to be noncatalytic for the dissociation reactions and fully catalytic for the ionization reactions. In this approach, a two-temperature dissociation model is used in generating the reacting flow behind the normal shock wave. This model equates the molecular rotational temperature to the kinetic temperature of the atoms and molecules, and also equates the electron kinetic and electronic temperatures to the molecular vibrational temperature. In the two-temperature model, all molecules have the same vibrational temperature, the degree of ionization is small, and the chemical reactions occur in the ground states of the atoms and molecules.

The computed temperature profiles are compared in Fig. 8. The two-temperature continuum approach provides a translation-rotation value, and a vibration-electron-electronic value. The particle DSMC approach provides separate values for the translational, rotational, and vibrational energy modes and equates the electronic temperature to the vibrational temperature to calculate the radiation.

The temperature profiles exhibit many differences. The DSMC solution shows considerable shock thickness and structure which is omitted in the continuum calculation. In the DSMC computation, there is a significant region of the shock where the translational and rotational modes are not equilibrated, thereby casting doubt on the validity of the continuum two-temperature approach at least at these low densities.

The rise in vibrational temperature predicted by DSMC is slower than that computed in the continuum simulation. Further, the DSMC method predicts a higher degree of nonequilibrium between the vibrational mode and the translational and rotational modes all along the stagnation streamline. The reasons for these differences in the two solutions are not clear at this point. The factors involved include differences in simulating viscosity, thermochemistry, and transforming a one-dimensional calculation into a stagnation streamline flow. These factors need to be investigated more thoroughly.

The mole fractions of atomic nitrogen and oxygen computed with the continuum method and the DSMC code for these conditions are compared in Fig. 9. Generally, the agreement is quite good except within the shock wave itself which is omitted in the con-

tinuum code. In the continuum technique, it is assumed that no chemical reactions occur upstream of the shock standoff location. The DSMC computation indicates that significant chemical activity does take place through the shock. This is due to the finite thickness of the shock-wave and to diffusion effects. Thus, the rise in atomic mole fractions computed by DSMC precedes the continuum results by a significant distance. The profiles computed by the two methods then follow similar paths until the last few centimeters next to the body, where the continuum code assumes the flow to be chemically frozen. The variation in mole fraction of N_2^+ computed with the two techniques is shown in Fig. 10. The rise in N_2^+ predicted by DSMC occurs in the thick shock-front and therefore leads the continuum solution. Behind the shock, the DSMC results provide a higher concentration of N_2^+ than the continuum data.

The spontaneous radiative emission profiles obtained from the continuum and DSMC solutions are compared in Fig. 11. The peak emission obtained with the new DSMC models is significantly lower than that computed with the continuum method, due to the smaller electronic (vibrational) temperature.

The integrated radiative heating at the stagnation point computed with the DSMC calculation is about 47 kW/m^2 while the continuum solution gives a value of 75.5 kW/m^2 . The contributions to the total radiative heating made by the various spectral regions are listed in Table 4.

Despite the large differences observed in the flow-field solutions, it is interesting to note that the continuum and DSMC total radiative heating estimates lie within a factor of 2 of each other. It is also worth noting that by increasing the shock standoff distance from 0.110 m (from Ref. 8) to 0.188 m (from Ref. 1) the total radiative heating predicted by the new DSMC thermochemistry models is doubled, indicating nearly linear scaling between these two quantities.

For the sake of completeness, the flow conditions investigated in Ref. 1 were also computed with the old DSMC thermochemistry models. The difference in flow quantities computed with the old and new models was similar to those shown in Figs. 4 through 6. The flow quantities were again interpreted in terms of total radiative heating at the stagnation point

using NEQAIR. The solution obtained with the old DSMC thermochemistry models gave a radiative heating which was ten times higher than that predicted with the new models.

Concluding Remarks

A new approach has been evaluated for predicting the radiative heating of a blunt-body entering the Earth's atmosphere. In this approach, the fluid mechanics of the flow along the stagnation streamline was predicted using a particle method (the direct simulation Monte Carlo method, DSMC), which is decoupled from the radiative emission.

Comparison was made with a previous DSMC calculation which employed outdated thermochemistry models together with a simplified, coupled radiation model. For the purpose of this comparison, the present DSMC computation also employed the old DSMC thermochemistry models. These two very different approaches gave agreement to within a factor of 2 for the total radiative heating at the stagnation point. This is viewed as acceptable considering the differences between the radiation models employed. The decoupled approach gave the higher value which was attributed in part to the absence of radiative cooling.

For the same flow conditions, the use of new DSMC thermochemistry models led to a decrease by a factor of 15 in the total radiative heating at the stagnation point. This drastic reduction in heating illustrates the sensitivity of the computed data to the physical models employed in the simulations. It is proposed that the new thermochemistry models, which have been successfully evaluated in previous studies, should provide more realistic simulation results. This decrease in radiative heating indicates that it is not necessary to couple radiation to the fluid mechanics under these flow conditions. To attain greater confidence in the numerical simulations, it is clear that experimental data is required for the validation of these physical phenomena.

A further comparison of the new DSMC chemistry models with a continuum calculation gave agreement within a factor of 2 for the total radiative heating, despite considerable differences in the flowfield solutions. The main conclusion of this study is that there remains a large degree of uncertainty in the application of state-of-the-art numerical methods for the pre-

diction of radiative heating to hypersonic vehicles flying in low-density regions of the Earth's atmosphere. Considering the importance of such heating to many future aerospace projects, there is a need for continued numerical and experimental investigation in this area.

Acknowledgement

Support (for I.D.B.) by NASA (Grant NCC2-582) is gratefully acknowledged.

Table 1. Freestream conditions.

Source	Altitude	U_∞ (m/s)	ρ_∞ (kg/m ³)
Ref. 8	78 km	9110	2.75×10^{-5}
Ref. 1	80 km	9756	2.05×10^{-5}

Table 2. Spectral regions analyzed with NEQAIR.

Region (μm)	Description	Absorption
0.1130-0.1140	N atomic lines	Yes
0.1160-0.1170	N atomic lines	Yes
0.1170-0.1180	N atomic lines	Yes
0.1195-0.1205	N atomic lines	Yes
0.1240-0.1250	N atomic lines	Yes
0.1294-0.1314	N and O atomic lines	Yes
0.1315-0.1325	N atomic lines	Yes
0.1323-0.1333	N atomic lines	Yes
0.1405-0.1415	N atomic lines	Yes
0.1490-0.1500	N atomic lines	Yes
0.1740-0.1750	N atomic lines	Yes
0.2000-2.0000	Molecular lines	No

Table 3. Total radiative heating (in kW/m²) using DSMC for the flow conditions from Ref. 8.

Region (μm)	Old Model	New Model
0.1130-0.1140	3.11	0.08
0.1160-0.1170	4.19	0.16
0.1170-0.1180	2.30	0.08
0.1195-0.1205	6.07	0.21
0.1240-0.1250	3.65	0.14
0.1294-0.1314	8.23	0.24
0.1315-0.1325	3.16	0.23
0.1323-0.1333	2.37	0.07
0.1405-0.1415	3.13	0.28
0.1490-0.1500	11.94	0.72
0.1740-0.1750	19.30	2.21
Sub-Total	67.5	4.42
0.2000-2.0000	272.2	19.0
Total	339.7	23.4

Table 4. Continuum and DSMC contributions (in kW/m²) of the various spectral regions to the total radiative heating at the stagnation point for the flow conditions from Ref. 1 at an altitude of 80 km.

Region (μm)	Continuum	New Model
0.1130-0.1140	0.44	0.20
0.1160-0.1170	0.76	0.50
0.1170-0.1180	0.32	0.27
0.1195-0.1205	0.84	0.46
0.1240-0.1250	0.92	0.40
0.1294-0.1314	0.76	1.13
0.1315-0.1325	0.76	0.61
0.1323-0.1333	0.52	0.19
0.1405-0.1415	0.84	0.70
0.1490-0.1500	2.84	1.65
0.1740-0.1750	5.36	4.73
Sub-Total	14.4	10.8
0.2000-2.0000	61.1	36.2
Total	75.5	47.0

References

- Whiting, E.E. and Park, C., "Radiative Heating at the Stagnation Point of the AFE Vehicle," NASA Technical Memorandum 102829, November 1990.
- Park, C., "Nonequilibrium Air Radiation (NEQAIR) Program: User's Manual," NASA Technical Memorandum 86707, 1985.
- Park, C., "On Convergence of Computation of Chemically Reacting Flows," AIAA Paper 85-0247, January 1985.
- Boyd, I.D., "Analysis of Vibration-Dissociation-Recombination Processes Behind Strong Shock Waves of Nitrogen," *Physics of Fluids A*, Vol. 4, No. 1, 1992, pp. 178-185.
- Boyd, I.D., "Analysis of Rotational Nonequilibrium in Standing Shock Waves of Nitrogen," *AIAA Journal*, Vol. 28, No. 11, 1990, pp. 1997-1999.
- Boyd, I.D., "Rotational and Vibrational Nonequilibrium Effects in Rarefied Hypersonic Flow," *Journal of Thermophysics and Heat Transfer*, Vol. 4, No. 4, 1990, pp. 478-484.
- Haas, B.L. and Boyd, I.D., "Models for Vibrationally-Favored Dissociation Applicable to a Particle Simulation," AIAA Paper 91-0774, AIAA 29th Aerospace Sciences Meeting, Reno, NV, January 1991.

⁸ Moss, J.N., Bird, G.A. and Dogra, V.K., "Nonequilibrium Thermal Radiation for an Aeroassist Flight Experiment Vehicle," AIAA Paper 88-0081, AIAA 26th Aerospace Sciences Meeting, Reno, NV, January 1988.

⁹ Boyd, I.D. and Gökçen, T., "Evaluation of Thermochemical Models for Particle and Continuum Simulations of Hypersonic Flow," AIAA Paper 92-2954, AIAA 27th Thermophysics Conference, Nashville, Tennessee, July 1992.

¹⁰ Park, C., "Assessment of Two-Temperature Kinetic Model for Ionizing Air," *Journal of Thermophysics and Heat Transfer*, Vol. 3, No. 3, 1989, pp. 233-244.

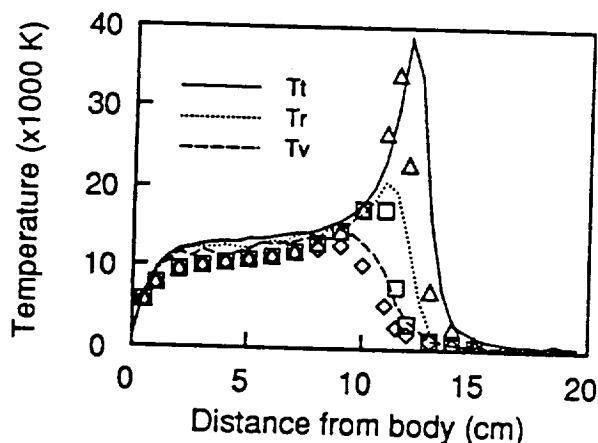


Fig. 1. Temperature profiles along the stagnation streamline: comparison of present calculations and Ref. 8 using the old DSMC thermochemistry models.

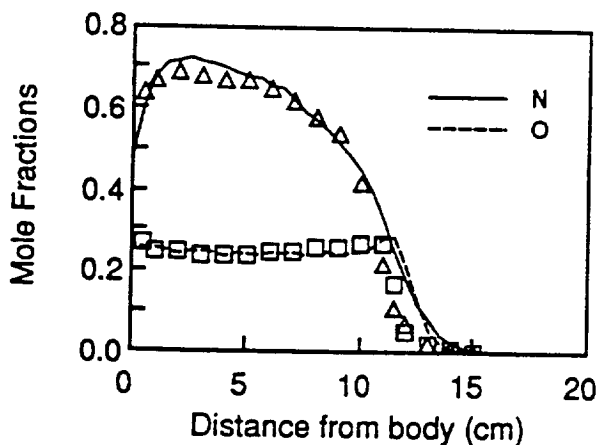


Fig. 2. Profiles of atomic species mole fractions: comparison of present calculations and Ref. 8 using the old DSMC thermochemistry models.

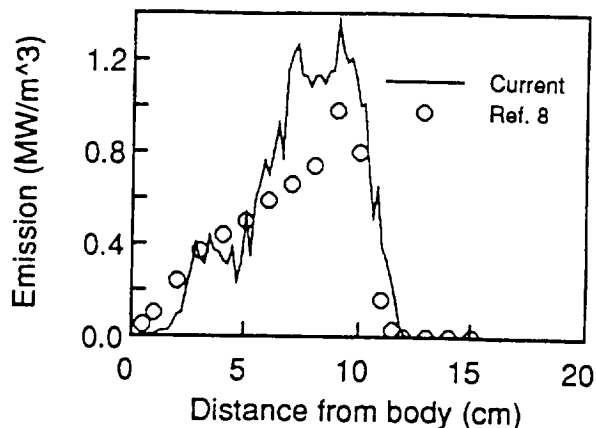


Fig. 3. Profiles of radiative emission along the stagnation streamline: comparison of present calculations and Ref. 8 using the old DSMC thermochemistry models.

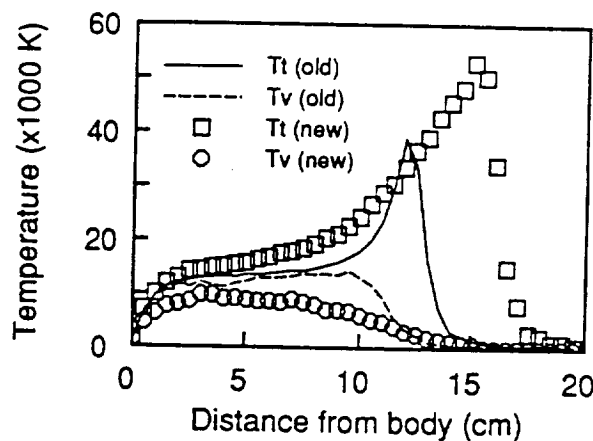


Fig. 4. Temperature profiles along the stagnation streamline: comparison of the old and new DSMC thermochemistry models.

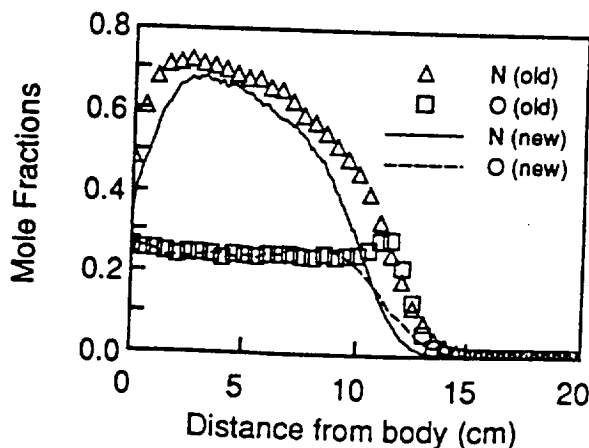


Fig. 5. Profiles of atomic species mole fractions along the stagnation streamline: comparison of the old and new DSMC thermochemistry models.

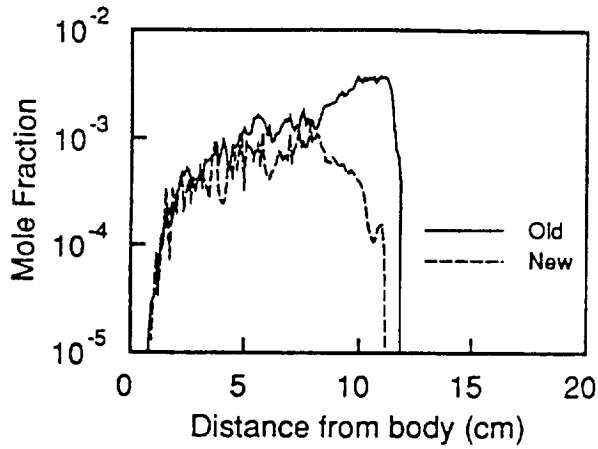


Fig. 6. Profiles of N_2^+ mole fraction along the stagnation streamline: comparison of the old and new DSMC thermochemistry models.

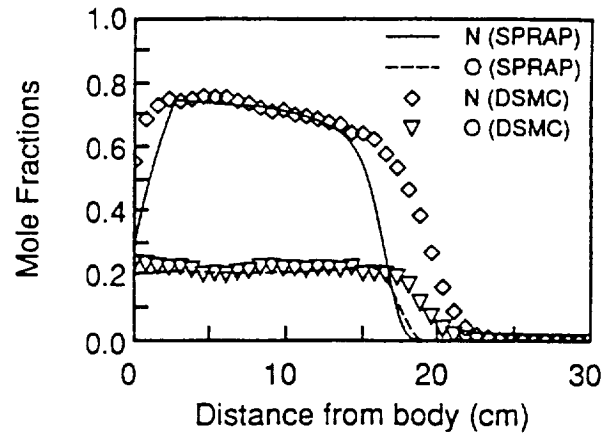


Fig. 9. Profiles of atomic species mole fractions: comparison of continuum and DSMC calculations using the new thermochemistry models.

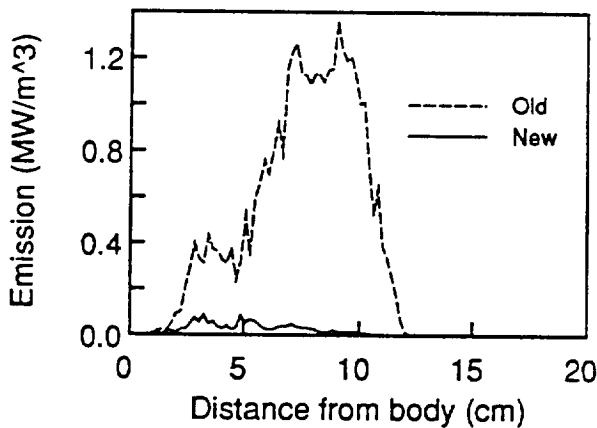


Fig. 7. Profiles of radiative emission along the stagnation streamline: comparison of the old and new DSMC thermochemistry models.

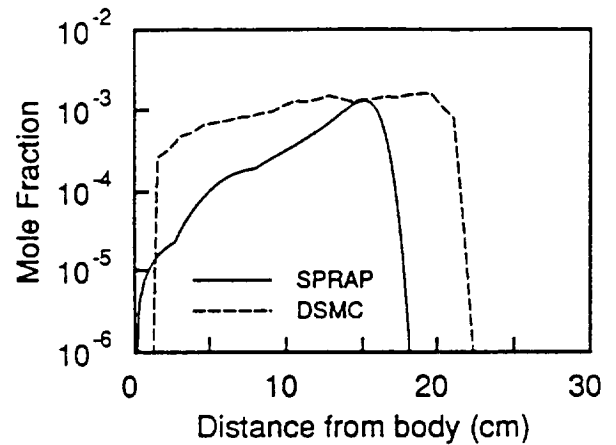


Fig. 10. Profiles of N_2^+ mole fractions: comparison of continuum and DSMC calculations using the new thermochemistry models.

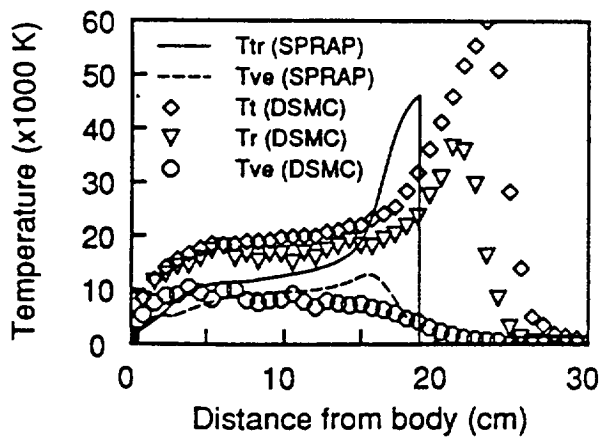


Fig. 8. Temperature profiles along the stagnation streamline: comparison of continuum and DSMC calculations using the new thermochemistry models.

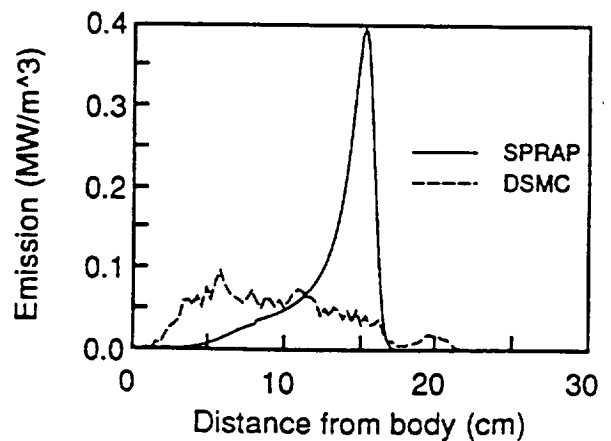


Fig. 11. Profiles of radiative emission: comparison of continuum and DSMC calculations using the new thermochemistry models.

APPENDIX D

SIMULATED PITCH, YAW, AND ROLL TORQUES ON THE MAGELLAN SPACECRAFT DURING AEROBRAKING

Brian L. Haas*

Eloret Institute, 3788 Fabian Way, Palo Alto, California 94303

Durwin Schmitt†

Martin Marietta Astronautics Corp., Denver, CO

Aerodynamic loads upon the Magellan spacecraft during proposed aerobraking through the atmosphere of Venus are computed at off-design attitudes with a direct Monte Carlo particle simulation method. This method is not restricted to the assumption of collisionless flow normally employed to assess spacecraft aerodynamics. Simulated rarefied flows at the nominal altitude of 140 km and entry speed of 8.6 km/s were compared to simulated and analytic free molecular results. The nominal spacecraft orientation is defined with the flow directed along the central body axis and perpendicular to the solar panels. Aerodynamic moments and lift for rarefied entry at several angles of pitch and yaw were at least 10% greater than free molecular results, while drag was about 20% lower. At each orientation, the resulting aerodynamic center of pressure on the body axis was located behind the vehicle center of gravity, providing restoring torques and promoting spacecraft stability. Roll torques about the body axis for entry at nominal orientation, but with the solar panels canted at various angles to the freestream flow, were computed and compared to free molecular results. This configuration has been suggested as an innovative experiment to assess gas-surface interaction during aerobraking. Periodic free-molecule boundary conditions and a coarse computational grid and body resolution served to minimize the simulation size and cost while maintaining solution accuracy.

NOMENCLATURE

n	number density
T	temperature
u	flow velocity
α	intermolecular potential exponent
ϵ	surface radiative emissivity
λ	gas mean free path
ρ	gas density

Subscripts:

s	stagnation value
∞	freestream value

INTRODUCTION

The Magellan spacecraft has been mapping the surface of Venus from a highly elliptic orbit (eccentricity, $e = 0.39$) since September of 1990. Mission planners at NASA's Jet Propulsion Laboratory (JPL) would like to circularize the orbit to improve mapping but cannot perform the maneuver through thruster activity alone due to limited remaining propellant. The orbital maneuver may be achieved through a series of gentle passes through the Venus atmosphere (1600 passes at $u = -1$ m/s each).¹ Besides circularizing the orbit, these maneuvers would provide considerable data related to atmospheric entry of satellite spacecraft.

The spacecraft configuration is depicted in Fig. 1 in its nominal entry orientation with flow directed (at orbit periapsis) along the central body axis. The solar panels in this configuration are normal to the flow, but indeed may be canted at any angle to form an effective "windmill" out of the spacecraft during entry. Restoring roll torques on the spacecraft may be measured along with surface heating and orbit altitudes to deduce the flowfield density and the surface accommodation coefficients in the normal and tangential directions. Axes for pitch and yaw are indicated in the front view.

Aerodynamic heating on the delicate solar panels during each aeropass was one mission constraint. Direct particle simulations of entry at several altitudes from 125 km to 140 km in the nominal orientation² verified that this heating was within the specified tolerance at altitudes exceeding 135 km. At the nominal altitude of 140 km, the heating and drag results corresponding to the rarefied flow were very close to those corresponding to free molecular (collisionless) flow at that altitude.

Mission planners are now concerned with spacecraft stability during aerobraking, particularly if the entry orientation has a high angle of pitch or yaw. Simplified analyses rely upon the assumption of free molecular flow which may not be valid at nominal flight conditions. The objective of the present study is to calculate body torques on the Magellan spacecraft for several entry orientations at the nominal entry altitude and periapsis velocity ($u_\infty = 8.6$ km/s), employing a particle simulation method which is not restricted to the free molecule flow assumption. The results of the rarefied simulation may then be compared to free molecu-

* Research Scientist, Member, AIAA.

Mailing Address: NASA Ames Research Center
M/S 230-2, Moffett Field, California 94035-1000

† Retired, Member, AIAA.

This paper is declared a work of the U.S. Government and is not subject to copyright protection in the United States.

lar results to assess the significance of molecular collisions in the flow. Roll torques associated with the windmill entry configurations were also computed at nominal conditions and compared to free molecule results. *The roll results are not presented in this abstract but will appear in the conference paper.*

PARTICLE SIMULATION METHOD

Direct simulation Monte Carlo (DSMC) particle methods model the motion and interaction of thousands or millions of computational particles to simulate gas dynamics.³ Specifics of the DSMC code employed in these studies are provided in Ref. 2. Given a particular position, velocity, and internal energy status, each particle in the flowfield travels unobstructed along the linear trajectory of its velocity vector over the duration of a single time step. At this time, neighboring particles are identified throughout the flowfield and paired-off as potential collision candidates. The flowfield is divided into a network of cells to facilitate identification of neighboring particles and to define the finest resolution for sampling macroscopic flow properties. Employing probabilities as functions of individual collision parameters such as collision cross-section and relative translational speed⁴, the subset of all candidate pairs which collide during the timestep are identified. In simulating free molecule flow, the probability of collision is artificially set to zero, representing an infinite molecular mean free path.

The entire simulated flowfield is initialized with free stream conditions. The particle simulation then runs through a transient phase as the solution develops and flowfield structures form. Upon reaching steady-state, the simulation collects statistical samples for measuring properties of the flowfield and body surfaces.

The code employed in the present study was developed by McDonald⁵ for efficient implementation on vector supercomputers. This code simulates non-reactive 3D flow of general gas mixtures about arbitrary geometries. Molecular collisions pertain to the Variable Hard Sphere model of Bird^{6,4} with an inverse intermolecular potential exponent of $\alpha = 5$. The internal energy modes are modeled with three fully-excited degrees of freedom to account for molecular rotation and vibration. Internal energy excitation is performed with the mechanics of Borgnakke and Larsen⁷ employing a fixed probability of relaxation of 1/5.

Body Geometry and Grid

The geometry of the Magellan spacecraft is shown in Fig. 1 and compared to the simulated geometry. Due to the large mean free path in the flow about the spacecraft, small features on the vehicle such as the altimeter antenna (ALTA), the medium and low gain antennas (MGA,LGA), and the rocket engine modules (REM) have negligible impact on the flowfield as a whole and may be excluded to simplify the simulation geometry, leading to two planes of symmetry on the vehicle.

To represent a surface in the cubic cartesian grid network of the simulation, it is necessary to approximate the surface as a composite of planar facets. Each facet has a normal defined from the intersections of the surface with the edges of the cell. This faceted description of the body is appropriate given that body radii are large in comparison to the cell size, and that the intersection of different surfaces occurs at cell boundaries. Since the solar panels are a dominant component of the structure, the simulation cell network was scaled such that the square simulated panels (measuring 8 cells \times 8 cells) have the same frontal area as the actual solar panels. This leads to the scaling factor, 1 cell = 31.44 cm. Such a coarse grid and body resolution was used in this study to reduce the computational expense associated with running several simulations.

Grid resolution greatly impacts the accuracy of solutions for vehicle aerodynamics and heating in rarefied flows. An established criterion for sufficient grid resolution is that the local mean free path must exceed the cell dimension. For cold-wall blunt-body rarefied flows, flowfield density will likely be quite large near the body surface, leading to small stagnation mean free paths. Simulated at nominal flight conditions, the flow density n and temperature T along the stagnation streamline at the center of the solar panel are plotted in Figs. 3 and 4. Equilibrium kinetic theory provides the following estimate of the local mean free path⁸ at the body surface,

$$\frac{\lambda}{\lambda_{\infty}} \approx \frac{n_{\infty}}{n} \left(\frac{T}{T_{\infty}} \right)^{2/\alpha} \quad (1)$$

At nominal conditions⁹ the freestream mean free path is $\lambda_{\infty} = 23.4$ m (74.43 cells). The stagnation properties lead to a stagnation mean free path around $\lambda_s \approx 4.2$ cells, exceeding the minimum accuracy criterion.

Body surfaces are modeled as if in radiative equilibrium with deep space at a temperature of 4 K and emissivity of $\epsilon = 0.82$, and employ a thermal accommodation coefficient of unity, typical of rough cool surfaces facing into the flow. This model is simple to implement in the simulation, it does not require a prescribed estimate of surface temperature, and it allows each surface facet to reach its own temperature independent of neighboring facets. It is assumed that radiation from the flowfield or from other body surfaces would contribute negligibly to the net heating of a given surface facet.

Flow Boundary Conditions

In simulating highly-rarefied flows, the computational flow domain must extend far enough upstream of the body to provide ample opportunity for freestream molecules to interact with those molecules that have reflected from the body and are diffusing upstream. Insufficient upstream domain size leads to overprediction of aerodynamic heating and forces.

Taking advantage of body symmetry, the simulated flowfield configuration is that of a wind tunnel depicted for pitch

simulations in Fig. 2 (100 L \times 120 H \times 12 W in cells) with a specularly-reflecting symmetry plane and a free-molecular outer plane. Particles which strike the outer plane after reflecting off of a body surface are removed from the flow field. All other particles striking the outer plane reflect specularly back into the flow. This effectively reduces the influence that the outer wall has upon the flow near the vehicle in highly-rarefied or free molecular flows.

Particles enter the flow domain from the left plane at the specified pitch angle, and exit normally from the right plane. The top and bottom planes represent free-molecular periodic boundary conditions. Again, particles which had reflected from the body before striking these planes are removed from the simulation. All other particles striking one of these planes simply re-enter the flow domain from the opposite plane, maintaining its original velocity vector. This boundary condition still provides freestream flow approaching the body geometry while reducing the required height of the wind tunnel, therefore minimizing the size and cost of the simulation.

SIMULATION RESULTS

Employing a freestream flow speed of $u_\infty = 8.6$ km/s and the day-side atmospheric data of Keating⁹ at 140 km altitude, simulations were performed for several entry orientations of pitch and yaw. Results from the particle simulation for rarefied flows, employing the finite molecular mean free path of $\lambda_\infty = 74.43$ cells, were compared to free molecular (collisionless) simulation results. These were, in turn, compared to analytic free molecular results generated with the FREEMAC code¹⁰ which employs ray-tracing algorithms to assess aerodynamic coefficients of spacecraft.

Limited computational resources and the large number of cases investigated in the present study restricted the number of particles which could be employed in the simulation to just four particles per cell in the freestream. However, density gradients in the flowfield significantly increased the particle densities near body surfaces such that 400,000 particles existed in the flowfield at steady-state. Employing roughly 4,000 transient steps and 6,000 steady-state sampling steps in the simulation, the number of statistical samples was sufficiently large to yield accurate and meaning solutions. Run-times averaged 1.0–2.0 CPU hours per case on the Cray-YMP supercomputer. The simulation could have employed ten times as many particles but would have required a ten-fold increase in computational time per case which was not warranted in the present study.

The simulation computes the net force and heat flux upon each surface facet of the vehicle. Torques are computed by the moments of body forces about a reference point defined by the intersection of the central body axis and the solar panel axis. This reference point is very close to the spacecraft center of mass. Moment coefficients are defined using the frontal area of the simulated geometry ($A_f = 236.8$ square cells), a reference length given by the HGA diameter ($D = 11.77$ cells), the freestream den-

sity ($\rho_\infty = 6.13 \times 10^{-9}$ kg/m³), and the freestream velocity.

The moment coefficients at each pitch attitude are given in Fig. 5. Note that the free molecular results from the particle simulation agree very well with FREEMAC results. Moment coefficients in the rarefied flow simulation, however, differ from free molecular results by as much as 40%. For all cases, the moment was directed so as to reduce the pitch of the vehicle. This was also observed in the yaw attitude cases plotted in Fig. 6. Again there is good agreement between the free molecule simulation and FREEMAC. *Rarefied yaw results were not available at the time of writing this abstract, but will appear in the conference paper.*

Aerodynamic lift and drag are plotted in Fig. 7 for the pitch cases. The limited data points available from FREEMAC agree very well with the particle simulation results for drag in free molecular flow, but flowfield collisions in the rarefied flow led to lower drag. Pitching the vehicle led to a downward force (negative lift) which was nearly twice as great in the rarefied flows than in the collisionless flows.

Finally, the location x_{cp} of the center of pressure behind the moment reference point on the central body axis is plotted in Fig. 8 for both pitch and yaw cases. At all attitudes, x_{cp} lies behind the center of gravity, promoting spacecraft static stability. Again, molecular collisions in the rarefied flows do have a noticeable effect upon x_{cp} .

The conference paper will include a comparison between FREEMAC results for the coarse geometry as used in the particle simulation, and a very fine geometry which closely resembles the actual spacecraft configuration. These results can be generated very quickly, but were not available at the time of writing this abstract.

CONCLUDING REMARKS

The aerodynamics of the Magellan spacecraft during proposed entry into the atmosphere of Venus may be computed for free molecular flows with the FREEMAC code. However, at the nominal altitude of 140 km, the free molecular flow assumption may no longer be valid. This study computed the body torques on the spacecraft when entering with various-off-design attitudes, using a direct particle simulation method for rarefied flow conditions. Repeating these simulations for collisionless flow provided a direct means of assessing the significance of molecular interactions in the flow, as well as providing a means to validate the technique through comparison to FREEMAC results. Use of a coarse body resolution permitted repeated inexpensive calculations without sacrificing solution accuracy. Results indicate that body torques will act to restore the vehicle to its nominal zero-pitch, zero-yaw attitude. The quantitative results of this study may facilitate assessment of spacecraft stability. Most importantly, this study demonstrates that the assumption of free molecular flow underpredicts the resulting body torques and lift, while overpredicting drag.

ACKNOWLEDGEMENTS

The authors gratefully acknowledge the assistance and technical support of Dr. Daniel Lyons (JPL), and the support of NASA-Ames Research Center for use of its facilities. This work is sponsored in part (for B.L.H.) by NASA grant NCC 2-582.

REFERENCES

¹ LYONS, D.T, SJOGREN, W., JOHNSON, W.T.K., SCHMITT, D. AND MCDONALD, A., "Aerobraking Magellan", *AAS Paper No. 91-420*, Durango, Colorado, Aug., 1991.

² HAAS, B.L. AND FEIEREISEN, W.J., "Particle Simulation of Rarefied Aeropass Maneuvers of the Magellan Spacecraft," *AIAA Paper No. 92-2923*, July 1992.

³ BIRD, G.A., *Molecular Gas Dynamics*, Clarendon Press, Oxford, 1976.

⁴ BAGANOFF, D. AND MCDONALD, J.D., "A Collision-Selection Rule for a Particle Simulation Method Suited to Vector Computers," *Physics of Fluids A*, Vol.2, 1990, pp. 1248-1259.

⁵ MCDONALD, J.D., "A Computationally Efficient Particle Simulation Method Suited To Vector Computer Architectures," Ph.D. Thesis, Stanford University, 1989.

⁶ BIRD, G.A., "Monte-Carlo Simulation In An Engineering Context," *Rarefied Gas Dynamics*, at 12th International Symposium on Rarefied Gas Dynamics, Charlottesville, VA, July, 1980.

⁷ BORGNAPPE, C. AND LARSEN, P.S., "Statistical collision model for Monte Carlo Simulation of Polyatomic Gas Mixture," *Journal of Computational Physics*, Vol.18, 1975, pp. 405.

⁸ BIRD, G.A., "Definition of mean free path for real gases," *Physics of Fluids*, Vol.26, 1983, pp. 3222-3223.

⁹ KLIJORE, A.J., MOROZ, V.I. AND KEATING, G.M., *Venus International Reference Atmosphere*, Vol. 5, No.11, 1986, pp. 142-148.

¹⁰ FREDO, R.M. AND KAPLAN, M.H., "Procedure for Obtaining Aerodynamic Properties of Spacecraft," *Journal of Spacecraft*, Vol.18, 1981, pp. 367-373.

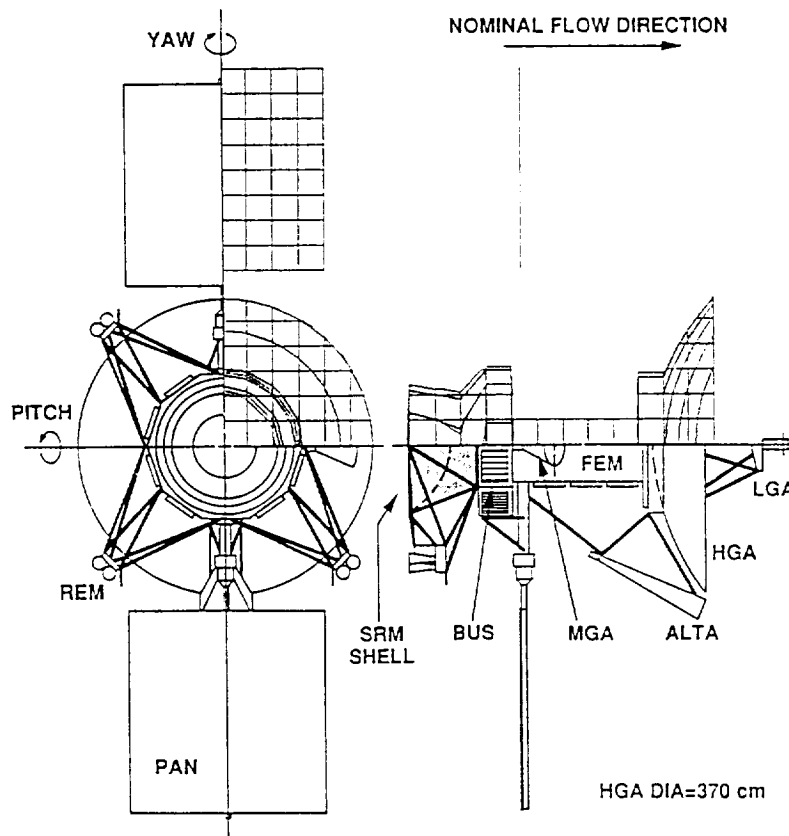


Fig. 1 Magellan spacecraft configuration versus simulated geometry shown at nominal attitude (zero pitch and yaw).

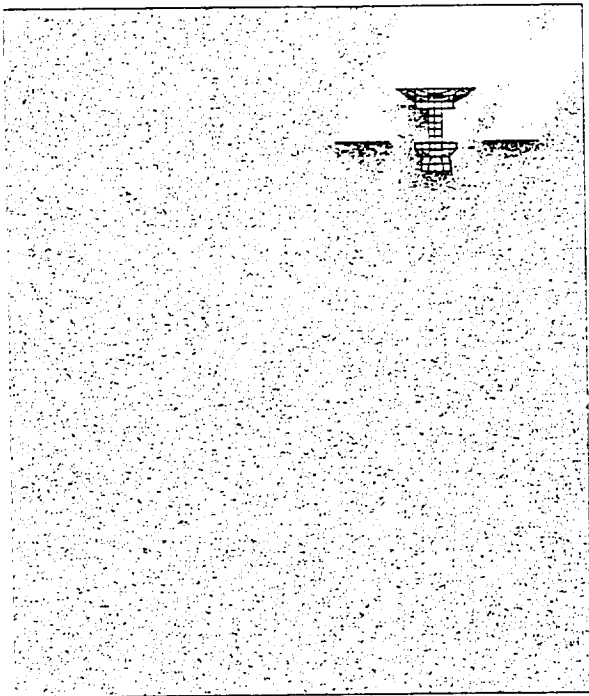


Fig. 2 Simulation geometry and flow domain for 30study. Wind tunnel measures 100 cells in length, up to 120 cells in height (for 45° study), and 12 cells in depth.

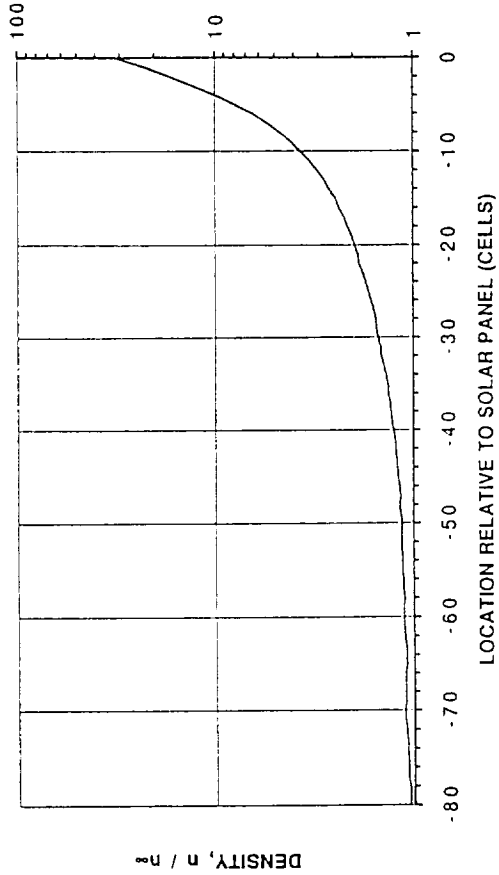


Fig. 3 Number density profile along the stagnation streamline ahead of the solar panel at its center (nominal attitude and flight conditions).

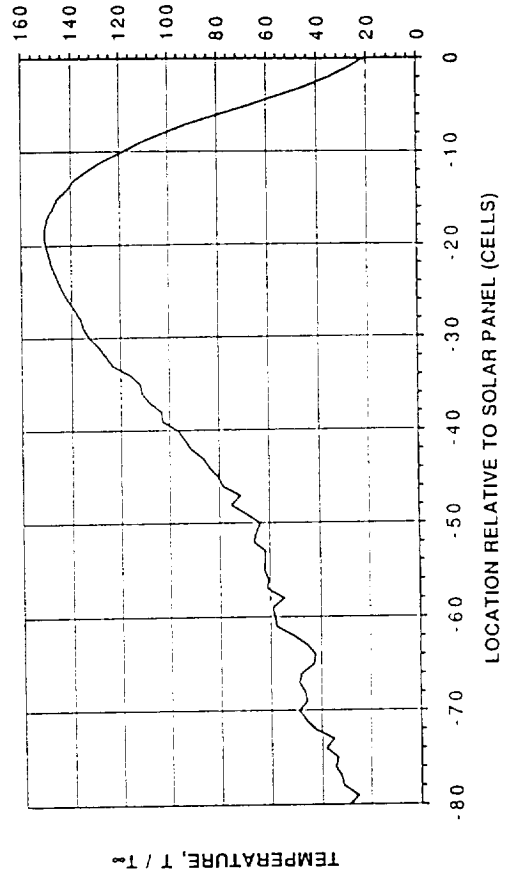


Fig. 4 Translational temperature profile along the stagnation streamline ahead of the solar panel at its center (nominal attitude and flight conditions).

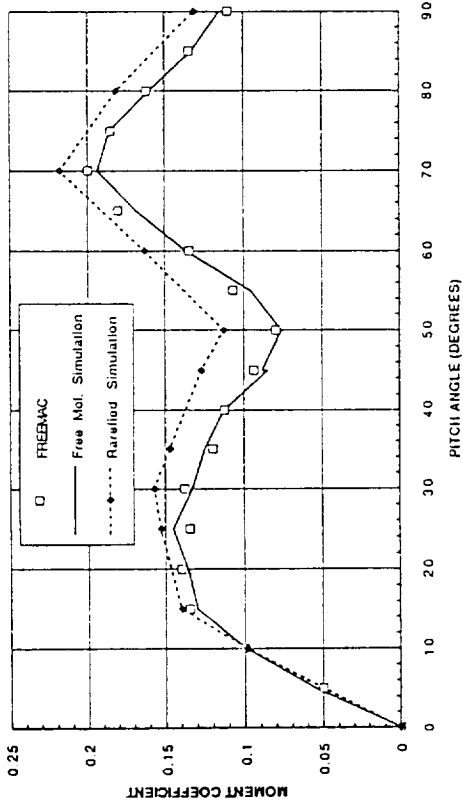


Fig. 5 Coefficient of restoring pitching moment for entry at various pitch angles. Comparison of rarefied and free molecular particle simulations results to FREEMAC results.

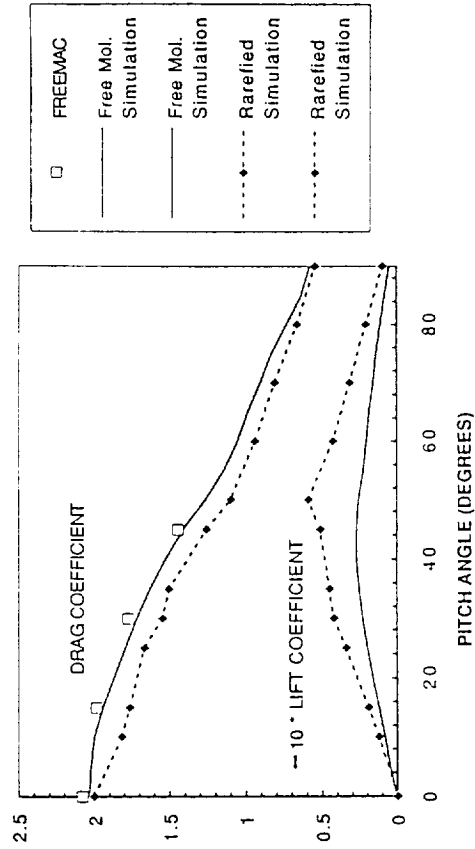


Fig. 7 Coefficients of drag and negative lift for entry at various pitch angles. Comparison of rarefied and free molecular particle simulations results.

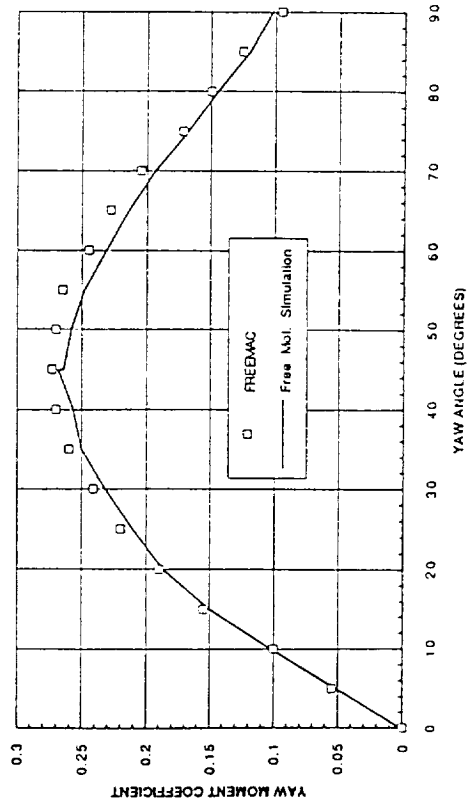


Fig. 6 Coefficient of restoring yaw moment for entry at various yaw angles. Comparison of free molecular particle simulations results to FREEMAC results.

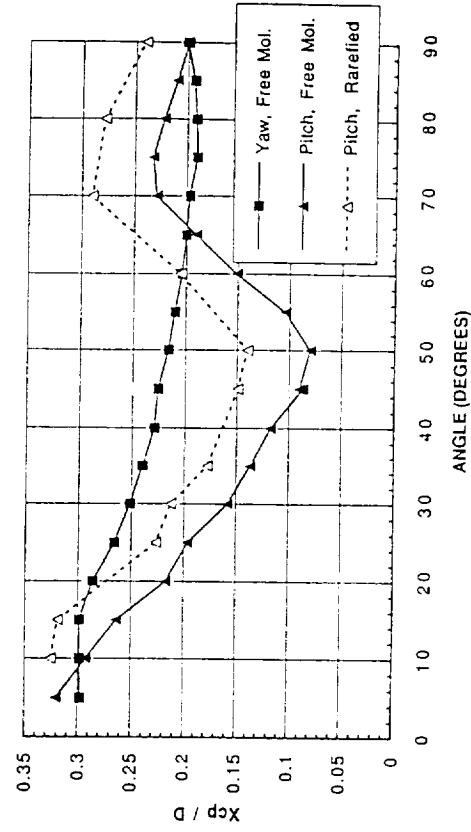


Fig. 8 Location of the center of pressure along the central body axis behind the reference point (approximate vehicle center of mass) for entry at various pitch and yaw attitudes. Comparison of rarefied and free molecular particle simulations results for pitch.

APPENDIX E

Particle Simulation of Satellite Aerobraking with Coupled Surface Heat Transfer

Brian L. Haas *

Elorot Institute, Palo Alto, California

Abstract

Models are developed for computing vehicle surface temperatures directly in a particle simulation of hypersonic rarefied flow. These models are validated through comparison of simulation results to experimental data and analytic solutions. Surface temperatures have a small yet noticeable effect upon vehicle aerodynamics and heating in rarefied flows. Multi-node thermal models accounting for transient convection, radiation, conduction, and heat capacity are appropriate for satellite aerobraking scenarios and may be implemented without additional computational burden to the simulation.

Introduction

Spacecraft may employ aerobraking to perform efficient orbital transfer maneuvers. However, most satellites are protected thermally by light blankets (if at all) rather than by heavy heat shields. As a result, they may fly only through the outermost reaches of the atmosphere where low flowfield densities lead to lower thermal and structural loading. Such aerobraking scenarios are characterized by high freestream Mach numbers M_∞ , high Knudsen numbers Kn_∞ , and short convective heating pulses $Q(t)$ possibly leading to transient surface temperatures. Aerobraking examples include two passes through Earth atmosphere by the Japanese HITEN satellite in March of 1991,¹ and circularization of the highly eccentric orbit of the Magellan spacecraft about Venus proposed for 1993.²

Highly rarefied flows may be computed by the direct simulation Monte Carlo (DSMC) technique^{3,4} in which the motion and interaction of many model particles simulate gas dynamics. These methods typically prescribe fixed surface temperatures when modeling gas-surface interactions. However, surface radiation, thermal conductivity within the spacecraft, and finite heat capacity of surface materials may each play a significant role in establishing surface temperatures during aerobraking. The objective of the present study is to develop surface heat transfer models which are coupled into the flowfield particle simulation to compute surface temperatures directly. The new models will be evaluated through comparison to experimental data and free-molecular flow theory. The effects of surface temperature upon vehicle aerodynamics will also be assessed.

Development of Surface Models

In particle methods, the simulated flowfield is divided into a network of small cells to facilitate collision modeling and statistical sampling. A vehicle geometry is approximated by a composite of planar facets in those cells intersected by body surfaces. In satellite aerobraking, these surfaces would be cold relative to the incident flow enthalpy and molecular diffusion into highly rarefied flows is

Copyright ©1992 by the American Institute of Aeronautics and Astronautics, Inc. All rights reserved.

* Research Scientist, Aerothermodynamics Branch, NASA Ames Research Center.

very sensitive to surface temperatures. Unless grazing the surface, most incident particles would accommodate fully to the surface and reflect diffusely with the corresponding surface temperature.

To compute surface temperatures, each surface facet is modeled as a single node in a thermal network. Prior to the aerobraking, all nodes are assumed to be in radiative equilibrium with deep-space at initial surface temperature T_o . Over time t during the heating pulse, each node i absorbs a transient convective heat flux due to incident particle collisions with the facet. The node reflects particles with surface temperature T_i , and radiates to deep-space at temperature T_o with emissivity ϵ_i . The net convection Q_i is the difference between incident and reflected heat fluxes per unit of surface area. Heat is conducted to neighboring nodes j with thermal conductivity $\kappa_{i,j}$ and to the isothermal spacecraft interior with conductivity $\kappa_{i,o}$. For simplicity, the invariant interior temperature will be assumed equal to the initial temperature T_o . The dynamic surface temperature of node i during the aerobraking heating pulse may be found by solving the energy conservation equation,

$$Q_i(t) - \epsilon_i \sigma (T_i^4 - T_o^4) - \kappa_{i,o} (T_i - T_o) - \sum_j \kappa_{i,j} (T_i - T_j) = c_i \frac{dT_i}{dt} \quad (1)$$

where $\sigma=5.67 \times 10^{-8}$ W/m²-K is the Stefan-Boltzmann constant and c_i is the heat capacity of the node. As employed here, κ and c already account for material thicknesses and densities.

Due to computational limitations, converged solutions in particle methods typically simulate aerobraking at a single point in time only, such as at perigee where peak convective heating occurs. To determine the appropriate surface temperature at perigee for each facet, it is necessary first to assume some surface temperature, then compute the peak convective heating $Q_{i,max}$ from the simulation directly, and then integrate Eq. (1) separately, employing an assumed form for the dynamic heating pulse $Q_i(t)/Q_{i,max}$. Using the new surface temperatures, the particle simulation may progress on to the next step toward a converged solution. This technique is stable and imposes negligible additional computational burden on the simulation.

Model Application and Validation

Several rarefied flows of a perfect diatomic gas ($\gamma=1.4$) about a two-dimensional circular cylinder were simulated with the particle method. Simulation specifications are listed in Tables 1 and 2. Note that different types of surfaces (Models A-D) may be simulated depending upon the parameters employed in Eq. (1). Taking advantage of symmetry, only flow about the top half of the cylinder is simulated. A repulsive power-law ($\alpha=8.33$) collision model⁴ was used for all cases.

Fixed Isothermal Surfaces (Model A)

Experiments of Laufer and McClellan,⁵ Dewey,⁶ and Vrebalovich⁷ studied heat transfer (Nusselt number, Nu_s) in rarefied flows past hot wire anemometers. Results of particle simulations, employing fixed isothermal temperatures ($T_i=T_o$) near the stagnation temperature T_s at $M_\infty=5$, are compared to the experimental data in Fig. 1. Excellent agreement throughout the range of Reynolds number Re_s

serves to validate the ability of the simulation to capture heat transfer correctly in rarefied flows. Viscosity and Re_s are determined from Kn_∞ , M_∞ , and T_s/T_i .⁸ Simulations were repeated at higher Mach numbers to study the effects of surface temperature upon body heating and forces. Considering only the top half of the cylinder, the force component F_\perp perpendicular to the freestream flow is plotted in Fig. 2a for $M_\infty=20$ and is very sensitive to low surface temperatures T_i for highly rarefied flows. It is this component which most influences lift and torque on asymmetric bodies. Net convective heating Q is also sensitive to surface temperature as shown in Fig. 2b.

Radiating Perfect Conductors (Model B)

The surface temperature of a perfect thermally-conducting cylinder in free molecular flow while radiating to deep space ($T_o=0K$) has been solved analytically by Abarbanel.⁹ Such a model may be applicable to exposed metal truss elements on aerobreaking spacecraft. Employing compatible parameters (Model B), free molecular flows ($Kn=\infty$) at several Mach numbers were simulated with the particle method. Results in Fig. 3 agree very well with the analytic solutions. In each case, the simulation summed Eq. (1) over all surface nodes to compute a single surface temperature ($T_i=T_j$) in closed form directly from the total convective heat flux to the cylinder. Repeating the simulation for rarefied flows ($Kn<\infty$) demonstrates that, as expected, flowfield molecular collisions reduce the convective heating of the cylinder and lead to lower surface temperatures T_i .

Radiating Insulated Surfaces (Model C)

Satellites protected by thermal blankets may be modeled in Eq. (1) with negligible thermal conductivity ($\kappa=0$) and heat capacity ($c=0$). Here, each insulated (adiabatic) surface facet independently attains radiative equilibrium with deep-space at $T_o=0K$. Free molecular flows over radiating insulated cylinders were simulated with the particle method using Model C. Temperature profiles over the cylinder surface are plotted in Fig. 4 and agree well with compatible analytic solutions.⁹ Notice that at high Mach numbers, the front of the body effectively shades the rear from convective heat flux. Diffusion at lower Mach numbers allows convection to reach the back side of the cylinder, leading to higher surface temperatures there. Profiles for rarefied flows at $Kn=\{0.1, 1.0\}$ were included in the figure at $M_\infty=20$. Note that molecular collisions reduce the surface temperature at the stagnation point while heated gas is able to flow around to the back side of the cylinder.

Dual-Node Surfaces (Model D)

Neglecting lateral thermal conductivity ($\kappa_{i,j}=0$), but accounting for heat conduction to the spacecraft interior and the heat capacity of the surface material, Eq. (1) leads to a dual-node thermal model for each surface facet i . This is representative of the surfaces of spacecraft instruments or solar panels exposed to the flowfield, and requires integration of Eq. (1) for transient temperatures of each surface facet during the heating pulse.

As an aerobreaking scenario, rarefied flow about a 2.0 m (dia.) cylinder at 116 km Earth altitude was simulated using surface Model D in the particle method. The form of the heating pulse $Q(t)/Q_{max}$ was taken from Abe¹ with a duration of $\tau=100$ sec. Each transient heating term from Eq. (1) is plotted in Fig. 5 near the stagnation point ($\theta=5.6^\circ$) along with transient surface temperatures T_i at various positions θ around the cylinder. Note that peak convective heating Q occurs at

perigee while peak surface temperatures occur shortly afterward due to non-zero heat capacity.

Temperature, force, and heating profiles at these perigee conditions are plotted in Fig. 6 for particle simulations employing models C and D. Although surface temperatures differ significantly between the two models, drag and heating results for each model are virtually identical. Consistent with the observations from simulations employing Model A, the component of force perpendicular to the freestream flow, F_\perp , demonstrates some sensitivity to surface temperature.

Sensitivity of surface temperatures to the heat transfer parameters c , κ , and τ , is demonstrated in Fig. 7 for $\theta=5.6^\circ$ at perigee conditions. Surface temperatures approach the initial value T_o when the heating pulse is short or the material heat capacity is large ($c/\tau \rightarrow \infty$). Likewise, they approach a limiting temperature T_i^* as $c/\tau \rightarrow 0$, where T_i^* is dependent upon conductivity $\kappa_{i,o}$ (Fig. 7b), varying between interior temperature T_o and radiating insulated temperature T_{ni} .

Conclusions

For satellites during aerobreaking, implementation of the heat transfer model of Eq. (1) in a particle simulation method permits direct assessment of surface temperature profiles rather than requiring prescribed isothermal estimates. As demonstrated here, surface temperatures do have a small yet noticeable effect upon vehicle aerodynamics and heat transfer in highly rarefied flows. Several types of surfaces (fixed isothermal, radiating perfect conductor, radiating insulated, and dual-node) were simulated and results were compared with experimental data or analytic solutions to validate the models. Most importantly, these models are very simple to implement without additional computational burden for the simulation.

Acknowledgements

This work is sponsored by NASA grant NCC2-582 with computational resources provided by the Numerical Aerodynamic Simulation (NAS) facility.

References

- 1 Abe, T., Kawaguchi, J., Saito, S., Ichikawa, T. and Uesugi, K., "World's First Cis-Lunar Aerobreak Experiment Preliminary Report of the Results", Inst. Navigation, 47th Ann. Meeting of Navigation and Exploration, Williamsburg, VA, June, 1991.
- 2 Lyons, D.T., Sjogren, W., Johnson, W.T.K., Schmitt, D. and McRonald, A., "Aerobreaking Magellan", *AAS Paper No. 91-420*, Durango, Colorado, Aug., 1991.
- 3 Bird, G.A., *Molecular Gas Dynamics*, Clarendon Press, Oxford, 1976.
- 4 Bagnoff, D. and McDonald, J.D., "A Collision-Selection Rule for a Particle Simulation Method Suited to Vector Computers," *Physics of Fluids A*, Vol. 2, No. 7, 1990, pp. 1248-1259.
- 5 Laufer, J. and McClellan, R., "Measurements of Heat Transfer from Fine Wires in Supersonic Flows," *Journal of Fluid Mechanics*, Vol. 1, No. 3, 1956, pp. 276-289.
- 6 Dewey, C.F., "Hot Wire Measurements in Low Reynolds Number Hypersonic Flows," *American Rocket Society Journal*, Vol. 31, No. 12, 1962, pp. 1709-1718.
- 7 Vrebalovich, T., "Heat Loss and Recovery Temperature of Fine Wires in Transonic Transition Flow," *Rarefied Gas Dynamics*, edited by C.L. Brundin, Vol. 2, Academic Press, New York/London, pp. 1205-1219, 1966.
- 8 Bird, G.A., "Definition of Mean Free Path for Real Gases," *Physics of Fluids*, Vol. 26, No. 11, 1983, pp. 3222-3223.
- 9 Abarbanel, S., "Radiative Heat Transfer in Free-Molecule Flow," *Journal of Aerospace Science*, Vol. 28, No. 4, 1961, pp. 299-307.

TABLE 1: Simulation Surface Models and Flowfield Specifications^a

Model	ϵ_i	c_i/τ	$\kappa_{i,o}$	$\kappa_{i,j}$	M_∞	Kn_∞^b	T_∞	T_o/T_∞^c
A	0	∞	∞	∞	(5, 10, 20)	(0.03 - 10, ∞)	200	(1 - 16)
B	0.8	0	0	∞	(3 - 20)	(0.1, 1, ∞)	200	0
C	0.8	0	0	0	(3 - 20)	(0.1, 1, ∞)	200	0
D	0.8	15	20	0	30	1	312	0.32

NOTE: c_i/τ and κ in units of $W/m^2 \cdot K$, T in Kelvin.

^a Freestream conditions denoted by subscript ∞ .

^b Knudsen number based on cylinder diameter, $Kn_\infty = \lambda_\infty/D$.

^c Deep-space temperature assumed equal to initial (interior) temperature ($T_o = T_o$).

TABLE 2: Flowfield Cell Resolution

Kn_∞	λ_∞^a	D	Domain ^b	n_∞^c
0.03	1.0	33.3	110 x 80	15
0.10	2.0	20.0	70 x 50	20
0.30	3.0	10.0	60 x 40	25
1.00	10.0	10.0	50 x 50	25
3.00	30.0	10.0	50 x 50	25
10.00	100.0	10.0	50 x 50	25
∞	∞	10.0	50 x 20	20

^a Mean free path λ_∞ and diameter D in uniform cubic cells

^b Domain dimensions (Length x Height) in cells.

^c Freestream number density (particles/cell).

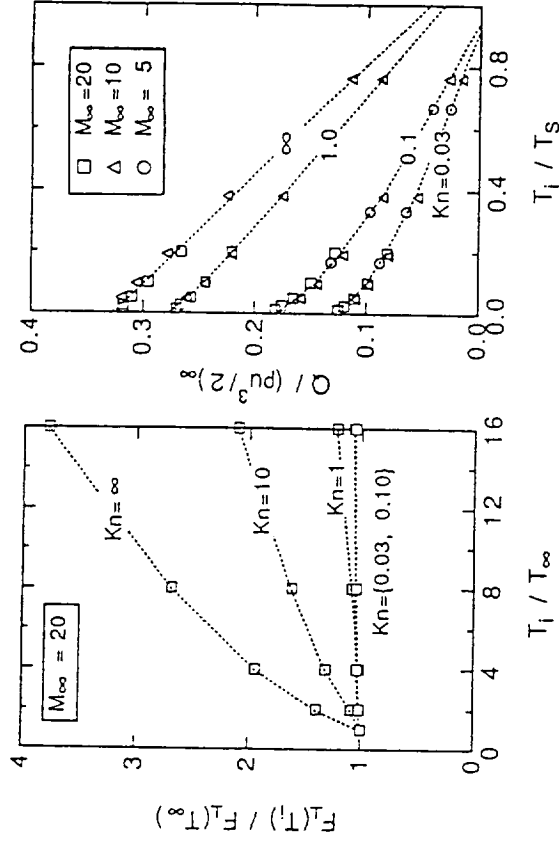


Fig. 2 Effects of surface temperature T_i and Knudsen number Kn_∞ upon: (a) aerodynamic force F_\perp perpendicular to freestream (each curve normalized by value at $T_i/T_\infty=1$), and (b) convective heating Q . Results of simulation employing fixed isothermal surfaces (Model A, $T_i=T_o$).

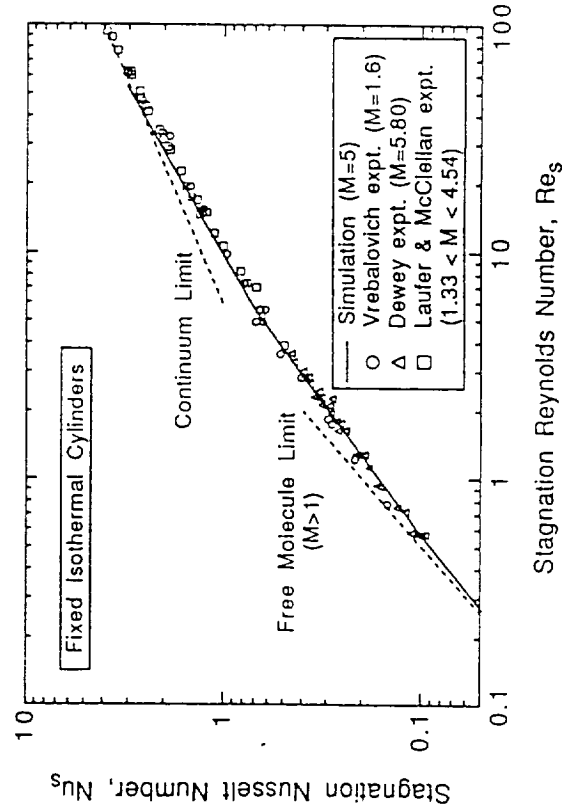


Fig. 1 Heat transfer for circular cylinders in rarefied flows. Comparison of experimental data to particle simulation results employing fixed isothermal surfaces (Model A). Nu_s and Re_s are defined from the cylinder diameter at stagnation conditions.

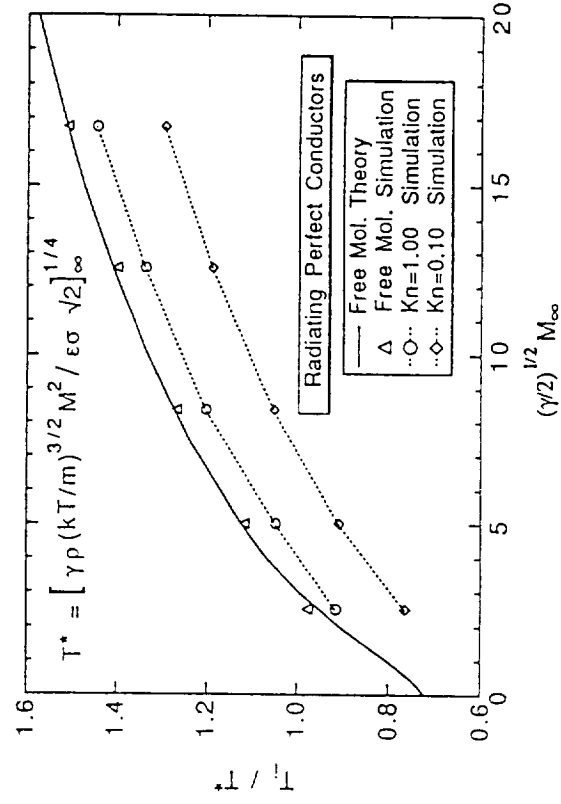


Fig. 3 Surface temperatures of radiating, perfectly-conducting cylinders in rarefied flows. Comparison of free molecular theory to simulation results employing Model B. T_i^* is evaluated at freestream conditions.

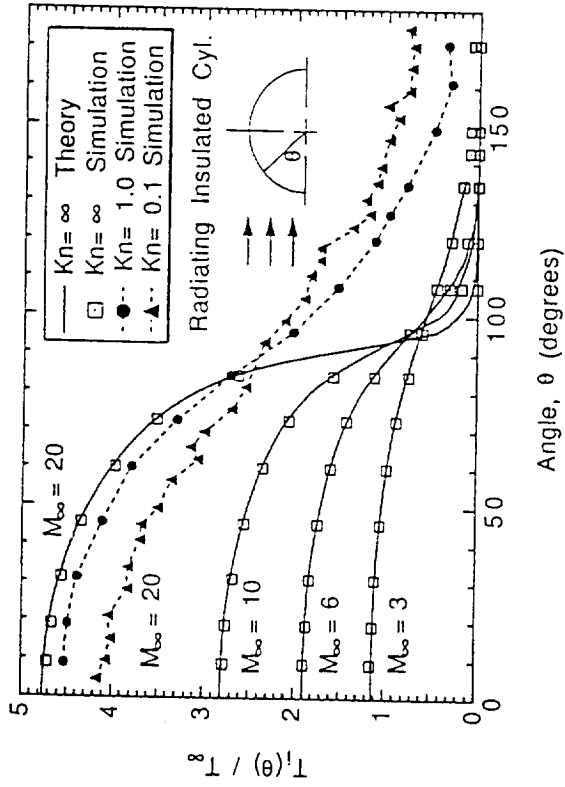


Fig. 4 Surface temperature profiles over radiating insulated cylinders in free molecular and rarefied flows. Comparison of free molecular theory to simulation results employing Model C and comparison of free molecular to rarefied flows at $M_\infty = 20$.

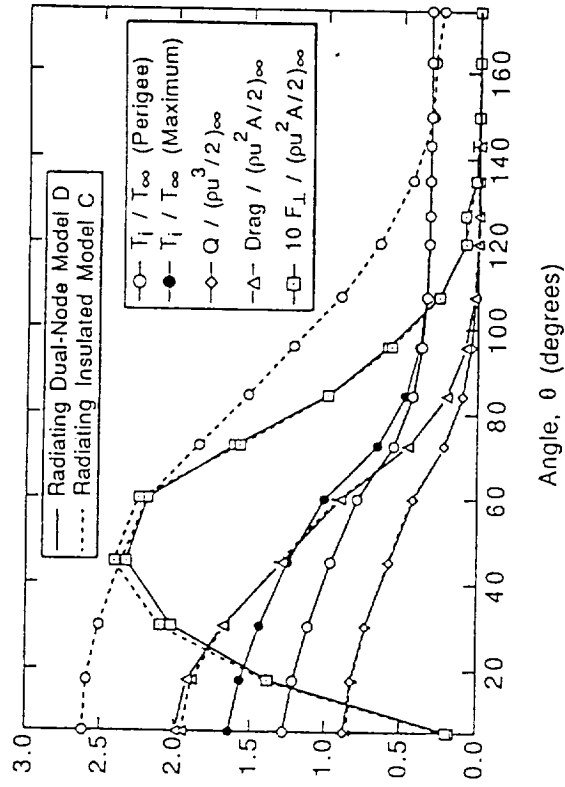


Fig. 6 Profiles of aerodynamic forces and temperatures along cylinder surface. Comparison of simulation results employing Model C and Model D.

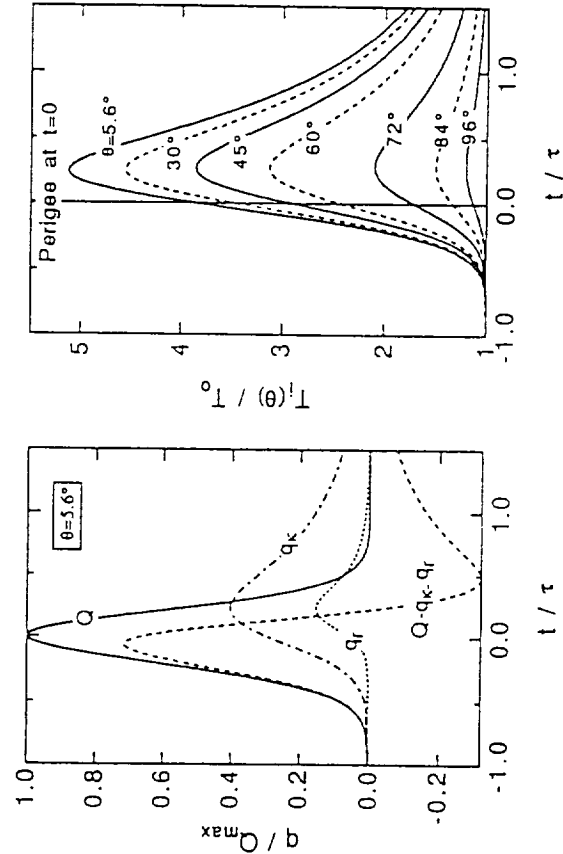


Fig. 5 Results of simulation employing dual-node model (Model D): (a) transient heating due to convection Q , conduction q_c , and radiation q_r ; and (b) transient temperatures at various locations on cylinder surface. Time is measured relative to perigee.

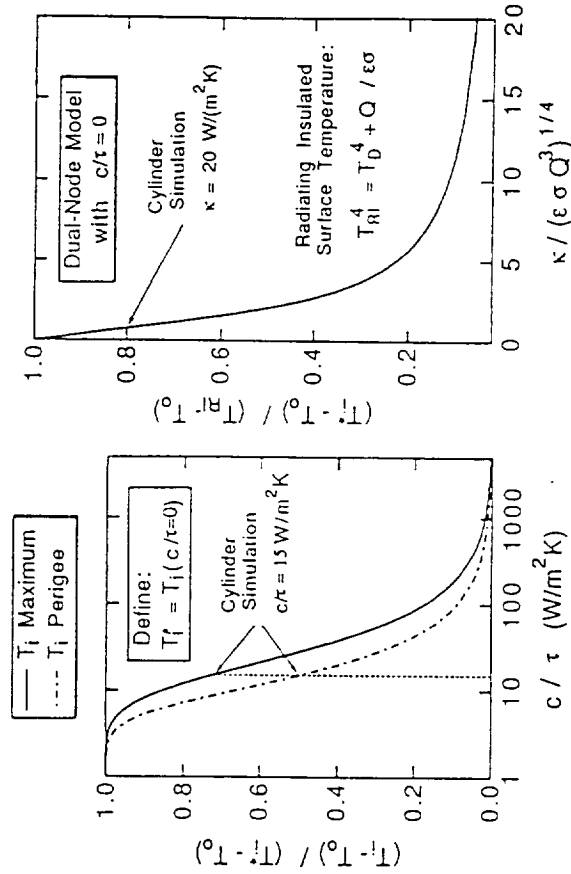


Fig. 7 Effects of heat transfer parameters c , τ and $\kappa_{i,\infty}$ upon surface temperatures for aerobraking using Model D at perigee conditions for $\theta = 5.6^\circ$. Define T_i as the limit when $c/\tau \rightarrow 0$, and T_{ii} as the radiating insulated limit.

APPENDIX F

FLOW RESOLUTION AND DOMAIN OF INFLUENCE IN RAREFIED HYPERSONIC BLUNT-BODY FLOWS

Brian L. Haas*

Eloret Institute, 3788 Fabian Way, Palo Alto, California 94303

A direct particle simulation method is used in this parametric study to assess the influence of upstream domain size and grid resolution upon flow properties and body aerodynamics in rarefied flows over cold blunt bodies. Insufficient grid resolution leads to over prediction of aerodynamic heating and drag, and underprediction of aerodynamic force perpendicular to the freestream flow direction. Solution accuracy within one percent error is attained when the grid cell size is no larger than roughly two molecular mean free paths near the body. Molecular diffusion from the body surface results in greater far-field domain influence as flow rarefaction increases. As a result, insufficient upstream domain size leads to overprediction of heating and drag along with underprediction of perpendicular force. However, since the use of short upstream domain size mimics free molecular flow, solution errors caused by the insufficient domain size are of less consequence as freestream rarefaction increases. Defining $x_{T_{max}}$ as the position ahead of the body where peak temperature occurs, this study shows that one percent error in solution accuracy is attained when the upstream computational domain size exceeds $3x_{T_{max}}$. Simulation of a hard-sphere gas is more sensitive to grid resolution while simulation of a Maxwell gas is more sensitive to upstream domain size.

NOMENCLATURE

D	cylinder diameter
F	aerodynamic force
Kn	Knudsen Number
L'	upstream domain size
M	Mach number
n	number density
q	aerodynamic total heat flux
T	temperature
x	location relative to stagnation point
α	intermolecular potential exponent
λ	gas mean free path

Subscripts:

s	stagnation value
w	wall value
x	in flow direction, drag
y	perpendicular to flow direction
∞	freestream value

INTRODUCTION

Flow field characteristics about blunt bodies during atmospheric entry lead to considerable challenges for computational simulation. Highly rarefied flows, where the gas density n is low and the mean free path λ between molecular collisions is high, are better suited to particle simulation methods, such as the direct simulation Monte Carlo (DSMC) technique pioneered by Bird,¹ rather than continuum techniques based upon the Navier-Stokes equations.

DSMC methods employ many model particles whose motion and interaction simulate gas dynamics directly. The simulated flowfield is divided into a network of small cells to facilitate collision modeling and statistical sampling. The computational burden of DSMC methods, however, grows proportionally with local gas density and the size of the computational domain. In typical entry flows, the body surface temperature is rather low compared to the stagnation temperature, leading to a steep density gradient near the body surface. Accurate simulation of this flow requires sufficient grid resolution near the body. Alternatively, the extent of freestream rarefaction results in a leading shock layer which is fully merged with the boundary layer of the body, yet extends far upstream. Accurate simulation therefore requires a large upstream computational flow domain. Together, these requirements rapidly drive the computational cost of the particle simulation method upward. The researcher must therefore understand what simulation costs are necessary to obtain a solution of sufficient accuracy. The objective of this parametric study is to assess quantitatively the sensitivity of aerodynamic loads and gas properties to grid resolution and simulation domain.

The present study employs an efficient particle simulation technique^{2,3} to investigate the net heat flux q and aerodynamic forces F on two-dimensional circular cylinders of diameter D , along with gas temperature T and number density n along the stagnation streamline, for hypersonic flows at Mach number $M_\infty = 20$ over the range of Knudsen numbers given by $Kn = \lambda/D = \{0.1, 0.3, 1.0, 3.0, 10.0\}$. The gas is modeled by hard-sphere particles with two fixed internal degrees of freedom. Interaction of the gas with the cylinder surface at wall temperature $T_w/T_s = 0.05$

* Research Scientist, Member, AIAA.
Mailing Address: NASA Ames Research Center
M/S 230-2, Moffett Field, California 94035

is modeled as fully diffuse and thermally accommodated, where T_s is the stagnation (total) temperature of the flow. All simulations employed between 10 and 20 particles per cell as the input freestream number density, n_∞ . For each set of conditions, the simulation resolution and domain were varied considerably and their effects upon solution accuracy were determined. Although not presented in this abstract, results for the conference paper will include studies at $M_\infty = \{5, 10\}$ and $T_w/T_o = \{0.1, 0.5, 1.0\}$.

In the DSMC technique, any two particles in the flow may collide only if they both reside in the same computational cell. Likewise, any two particles within a given cell can collide regardless of their respective positions in the cell. If the cell dimension near the cold body surface is too large, then energetic particles at the far edge of the cell are able to readily transmit momentum and energy to particles immediately adjacent to the surface. The latter particles may, in turn, transmit that energy and momentum to the surface. This leads to over-prediction of both the surface heat flux and the aerodynamic force on the body than would occur in the real gas. This error is minimized by reducing the cell dimension relative to the local mean free path of molecules near the surface. From kinetic theory, the local mean free path λ is related to the local number density n and temperature T as follows,

$$\frac{\lambda}{\lambda_\infty} = \left(\frac{n_\infty}{n}\right) \left(\frac{T}{T_\infty}\right)^{2/\alpha}, \quad (1)$$

where subscript ∞ denotes values at freestream conditions, and α is the exponent of the assumed inverse-power intermolecular potential which may vary between the limits of the Maxwell molecule ($\alpha = 4$) and the hard sphere ($\alpha = \infty$).

As a consequence of Eq. (1), regions of high density lead to short mean free paths, requiring finer cell resolution to capture flow gradients accurately. Density profiles along the stagnation streamline for the cylinder flows above are plotted in Fig. 1. Note that the density at the cylinder surface (at $x/D = 0$) is significantly higher than the freestream value. This behavior is more pronounced, and the gradients are steeper, for flows at lower Kn_∞ . This, combined with the fact that lower Kn_∞ means that the freestream λ_∞ is short, dictates that the cell resolution must be very fine compared to more rarefied flows.

Temperature profiles along the stagnation streamline for these same flows are also plotted in Fig. 1. These curves clearly demonstrate how far upstream of the body its presence affects the flow. This domain of influence increases with Kn_∞ as a result of upstream diffusion of particles which reflected from the body surface.

Flow density and temperature at the stagnation point on the cylinder may be used in Eq. (1) to determine the stagnation mean free path λ_s . As measured in units of cell-lengths, λ_s is dependent upon the cylinder diameters D employed in the simulations and is plotted for each Kn_∞ flow in Fig. 2.

The plot in Fig. 3 compares the local Knudsen number along the stagnation streamline for a Maxwell-molecule gas

and a hard-sphere gas. The gradients for the hard-sphere are steeper and lead to lower Kn at the stagnation point on the body compared to the Maxwell-molecule. Alternatively, the domain of influence extends much further upstream for the Maxwell-molecule. As a consequence, accurate DSMC solutions for hard-sphere gases require finer cell resolution while solutions for Maxwell-molecule gases require larger upstream computational fields.

For each of the flow conditions above, the grid resolution is defined by the cylinder diameter D while the flow domain size is defined by the distance L' of the computational field upstream of the cylinder. These length scales are depicted schematically in Fig. 4 along with $x_{T_{\max}}$ which represents the position of the peak temperature along the stagnation streamline upstream of the cylinder.

GRID RESOLUTION STUDY

For rarefied flows in the lower Knudsen number range $0.1 \leq \text{Kn} \leq 1.0$, simulations were performed to assess the effects of grid resolution upon solution accuracy. At each value of Kn_∞ , the flow was simulated using several grid-resolutions corresponding to cylinder diameters of $D = \{5, 10, 20, 30, 50, 100, 200\}$ cells-lengths. For all cases, a sufficient upstream domain size was used ($L'/D = 2$).

The density and temperature profiles along the stagnation streamline ahead of the body are plotted for $\text{Kn}_\infty = 0.1$ in Fig. 5. For the coarse grids, where $D < 50$ cells, the profiles were smeared considerably. For $D \geq 50$, the profiles coalesced to a single form and are therefore assumed to represent accurate solutions. This same general behavior was observed for the other Kn cases, although the resolution required to capture the appropriate profiles did not need to be as fine as in the $\text{Kn}_\infty = 0.1$ flow. Indeed, for $\text{Kn}_\infty = 1.0$, accurate profiles were obtained at $D \geq 20$.

For each simulation, the aerodynamic heating q and forces F_x and F_y were computed. Here, F_x represents drag force in the direction of the freestream flow. F_y is the net force, perpendicular to the freestream flow, on the top half of the body only. Note that the net lift force, integrated over the top and bottom halves of any axisymmetric body, would equate to zero.

To assess the error corresponding to a given flow resolution, the body aerodynamics computed with the finest resolution at each Kn value was assumed to represent the "correct" solution for that flow. Employing the stagnation density and temperature from that solution, the stagnation mean free path, λ_s , is determined from Eq. (1) for each resolution case and plotted in Fig. 2. Errors in body aerodynamics are plotted against λ_s for all cases in Fig. 6. At all resolutions, heating and drag were overpredicted while F_y was underpredicted (the absolute value of its error is plotted in the figure). These errors correlate fairly well with λ_s . Note that errors in heating are worse than errors in the forces (which are roughly equal but opposite). These plots indicate that aerodynamic errors will be less than one percent for grids in which the stagnation mean free path is on the

order of a half-cell or greater, regardless of the freestream rarefaction Kn_∞ . This conclusion, summarized by

$$\lambda_s \geq 0.5 \text{ cells} \quad \text{--Resolution Criterion} \quad (2)$$

represents an appropriate design-criterion for grid resolution in cold-wall blunt-body simulations.

FLOW DOMAIN STUDY

For rarefied flows in the higher Knudsen number range ($1.0 \leq Kn \leq 10.0$), simulations were performed to assess the influence of the upstream flow field domain upon solution accuracy. In view of the results above, the cell resolution used in each case here was sufficiently fine such that the stagnation mean free path was roughly one cell-length near the body. All cases employed the hard-sphere molecular model. The objective here was to employ different upstream computational field sizes, defined by length L' in Fig. 4, to determine the minimum acceptable domain size required for a given penalty in solution accuracy.

Flow density and temperature along the stagnation streamline is plotted in Fig. 7 at $Kn_\infty = 1.0$ employing different domain sizes L' . With sufficiently large L' , all the curves coalesced to a single curve to represent the assumed correct profile as represented at $L'/D = 4.0$. With insufficient upstream domain (i.e. L' is small), density is underpredicted while temperature is overpredicted. However, once the domain size that is used exceeds about twice the distance of the peak temperature location $x_{T_{max}}$, the temperature and density profiles followed the expected forms predicted when ample upstream domain was employed. This is observed in Fig. 7 at $L'/D = 0.7$. It is somewhat surprising that, although the flow was not simulated further upstream, the profiles matched the correct form as if it were. Though not presented here, behavior for flows at other Kn_∞ are qualitatively similar to the results above.

Quantitative assessment of the errors in aerodynamic loads on the cylinder for simulations employing different upstream domain sizes are presented in Fig. 8. The errors for each case are computed relative to the aerodynamic loads which were obtained using the largest domain L' and presumably represent the correct values. Each plot employs a length scale normalized by $x_{T_{max}}$. As expected, the errors in predicted aerodynamics decrease as larger upstream domain sizes are used. Aerodynamic heating q and drag force F_x were overpredicted in all cases while the force perpendicular to the freestream flow direction, F_y , was underpredicted.

Note that each curve begins to level off as $L'/x_{T_{max}}$ drops below roughly 0.3. In the limit of decreasing upstream domain, the incoming flow is almost completely unaffected by particles reflecting from the cylinder surface such that the aerodynamic loads approach the values corresponding to the free molecular flow limit. For heating and drag, the limit is less erroneous for flows at greater freestream Knudsen numbers Kn_∞ since free molecular flow represents the limit of greatest possible rarefaction.

The interesting paradox which has developed is that, while the domain of upstream influence increases with Kn_∞ , the computational penalty in terms of solution accuracy is less dramatic compared to simulations at lower Kn_∞ . Regardless, an appropriate criterion for defining a suitable computational flow domain for rarefied flow simulation is given by

$$L'/x_{T_{max}} > 3. \quad \text{Domain Criterion} \quad (3)$$

CONCLUDING REMARKS

When employing direct particle simulation methods, accurate simulation of highly rarefied flows about cold blunt bodies requires sufficient computational grid resolution and upstream flow domain size. The objectives of this parametric study were to assess quantitatively what penalty is suffered in solution accuracy when minimizing computational expense by using short domains and coarse grids. Qualitative results were similar for all freestream Knudsen numbers. Solution errors on the order of one percent for aerodynamic heating and forces are attained with grids for which the molecular mean free path near the stagnation point exceeds a half-cell in length while the upstream domain size exceeds three times the distance to the peak temperature point along the stagnation streamline. Simulated hard-sphere gases are more sensitive to grid resolution than Maxwell gases, but require less extensive upstream domains. The results presented in this abstract required less than two weeks to generate and will be duplicated in the final paper to include solutions at other freestream Mach numbers and surface temperatures.

ACKNOWLEDGEMENTS

The author would like to thank Dr. Wahid Hermina (Sandia National Laboratory) and Michael Fallavollita (Stanford University) for helpful discussions which led to this parametric study. The author acknowledges and appreciates the support of NASA-Ames Research Center and the Numerical Aerodynamic Simulation for use of their facilities. This work is sponsored by NASA grant NCC2-582.

REFERENCES

- ¹ BIRD, G.A., *Molecular Gas Dynamics*, Clarendon Press, Oxford, 1976.
- ² BAGANOFF, D. AND McDONALD, J.D., "A Collision-Selection Rule for a Particle Simulation Method Suited to Vector Computers," *Physics of Fluids A*, Vol.2, No. 7, 1990, pp. 1248-1259.
- ³ McDONALD, J.D., "A Computationally-Efficient Particle Simulation Method Suited to Vector Computer Architectures," Ph.D. Thesis, Dept. of Aeronautics and Astronautics, Stanford University, 1989.

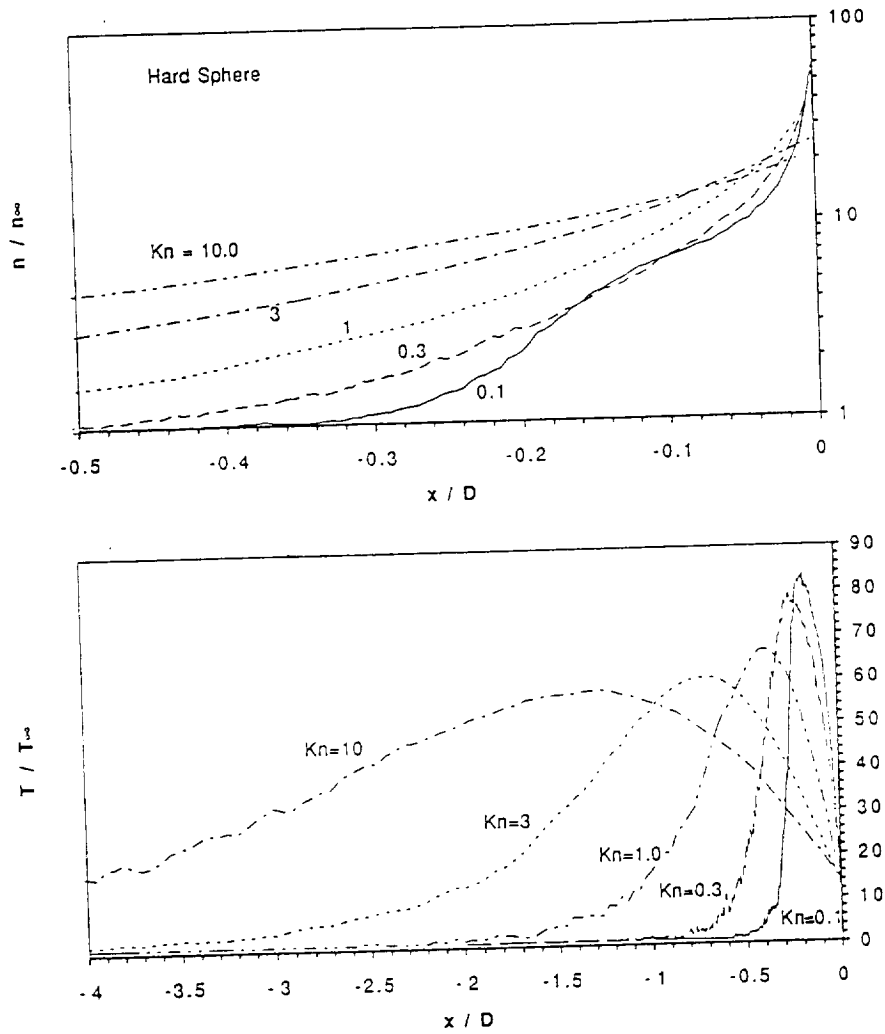


Fig. 1 Profiles along the stagnation streamline for flows of differing rarefaction at $M_\infty = 20$ over cold cylinders; (a) number density, n ; (b) temperature, T .

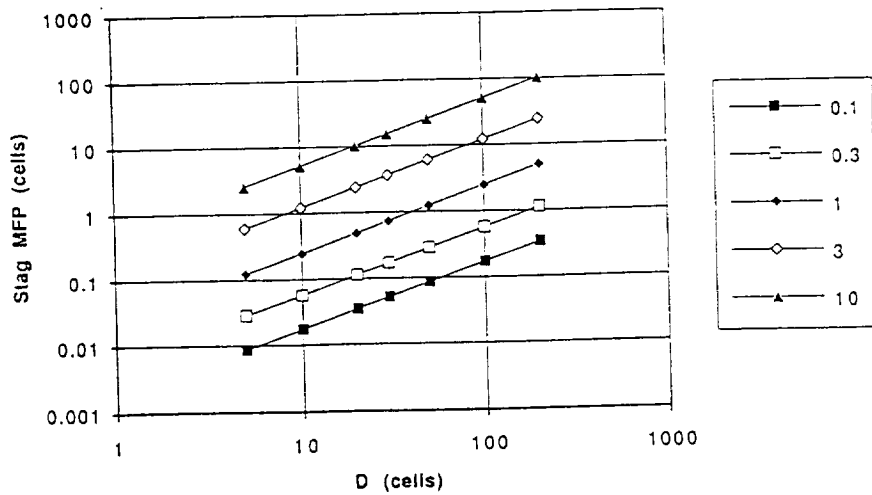


Fig. 2 Molecular mean free path at the stagnation point of the cylinder of diameter D (both measured in units of cell-lengths) for freestream Knudsen numbers, $0.1 \leq Kn_\infty \leq 10$ at $M_\infty = 20$ and $T_w/T_s = 0.05$.

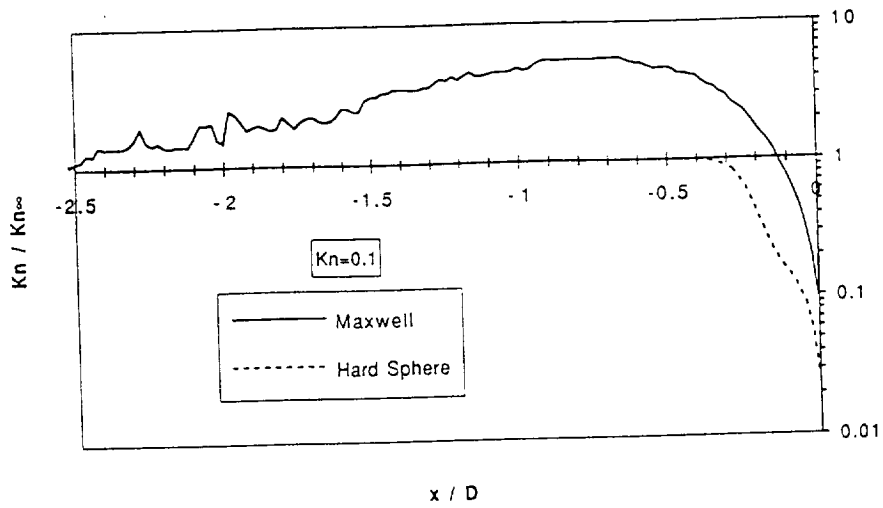


Fig. 3 Local Knudsen number along the stagnation streamline upstream of a cold cylinder for hard-sphere and Maxwell gases at $Kn_\infty = 0.1$.

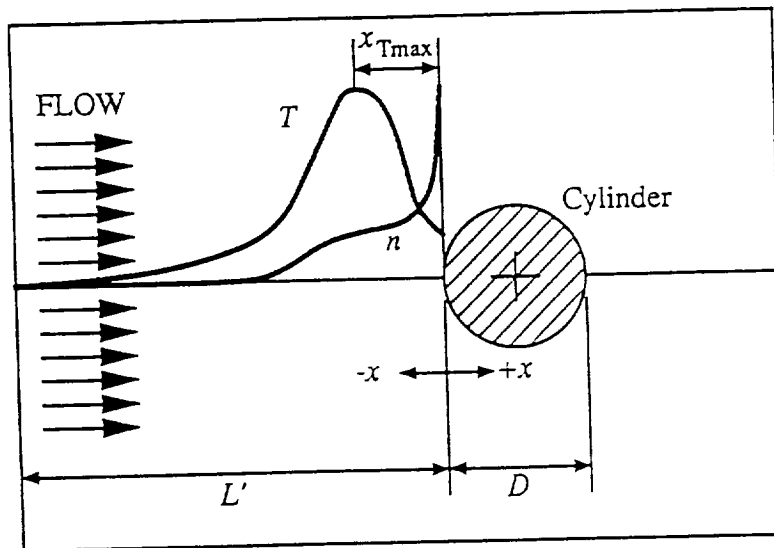


Fig. 4 Definition of simulation length-scales and schematic representation of temperature and density profiles upstream of a cold cylinder of diameter D in rarefied flow.

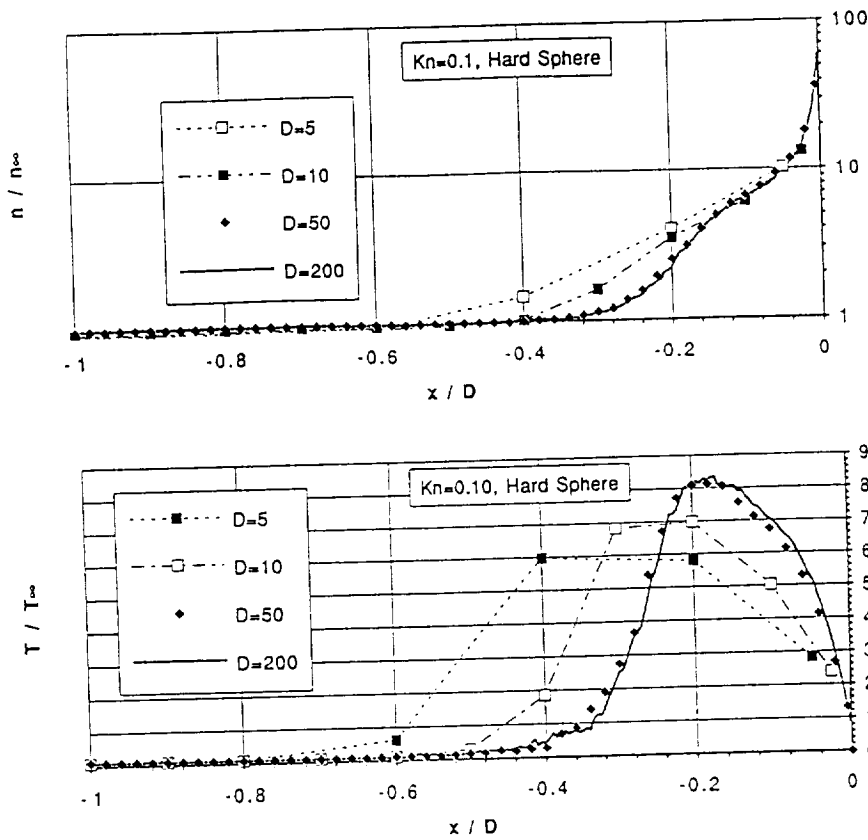


Fig. 5 Profiles along the stagnation streamline upstream of a cold cylinder for flows simulated at different grid resolutions for $Kn_\infty = 0.1$; (a) number density, n ; (b) temperature, T .

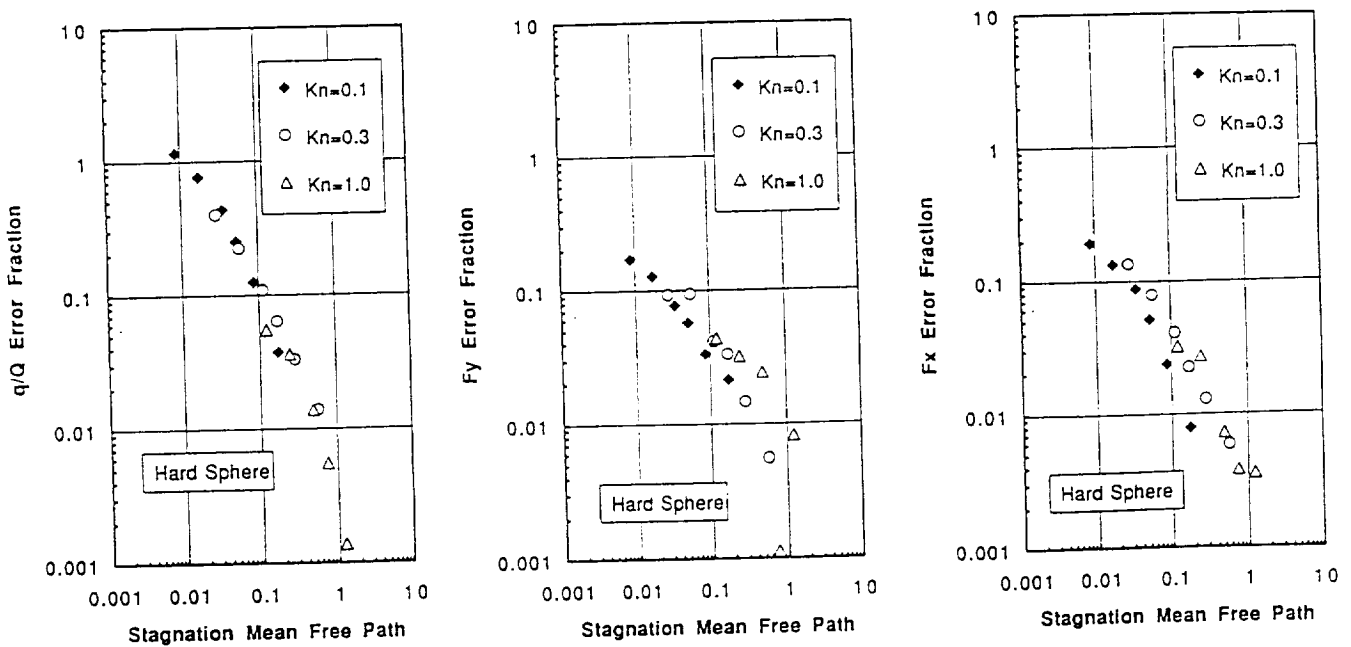


Fig. 6 Errors in aerodynamic loads upon a cold cylinder for flows simulated at different grid resolutions; (a) heating, q ; (b) drag force, F_x ; (c) perpendicular force, F_y . Absolute values of error fractions measured relative to loads computed at the finest resolutions.

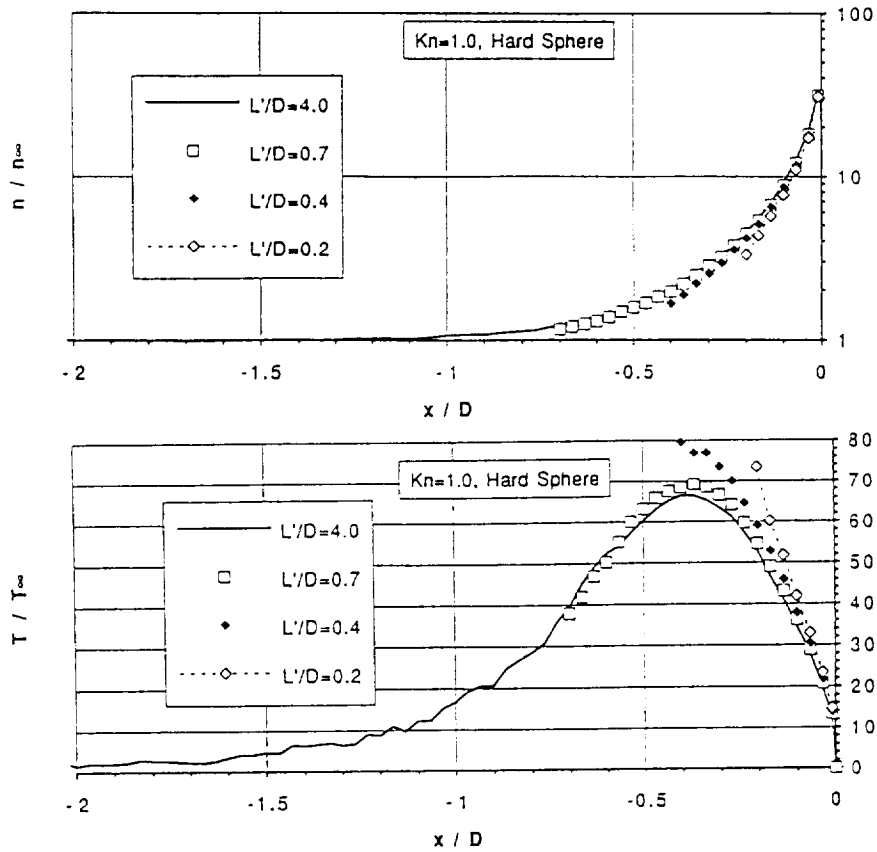


Fig. 7 Profiles along the stagnation streamline upstream of a cold cylinder for flows simulated with different upstream domain sizes for $Kn_{\infty} = 1.0$; (a) number density, n ; (b) temperature, T .

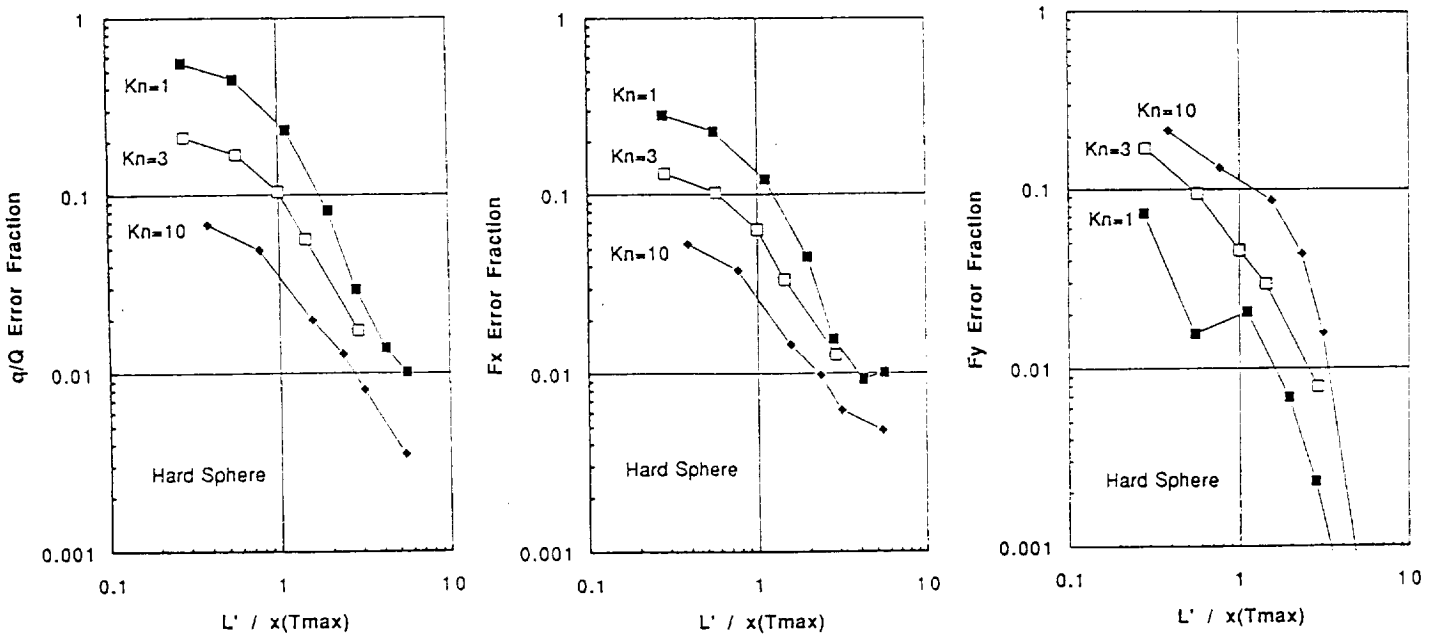


Fig. 8 Errors in aerodynamic loads upon a cold cylinder for flows simulated with different upstream domain sizes; (a) heating, q ; (b) drag force, F_x ; (c) perpendicular force, F_y . Absolute values of error fractions measured relative to loads computed with the largest domains.